an *in vitro* study using cultured rat microglia [8, 9]. We further showed that microglial transplantation increased Aβ clearance in Aβ-injected rats in an *in vivo* study [10]. Moreover, immunization with Aβ peptides in transgenic mouse models of AD effectively reduced brain Aβ and restored cognitive functions [11–14]. These reports suggest that immune systems in the brain, including microglia, may be involved in Aβ clearance in AD. However, our search of literature found no report that describes detailed temporal changes of microglia in response to the pathological changes in AD transgenic mice.

On the other hand, chronic nicotine treatment has been reported to reduce Aβ in the brains of AD model mice [15, 16], and normal elderly individuals who smoke have been found to have less Aβ deposits in the brain [17]. Recent studies have reported that microglia also express alpha 7 nicotinic acetylcholine receptor (α7 nAChR) [18, 19]. We previously confirmed that treatment of rat microglia with galantamine (an acetylcholinesterase inhibitor and also an allosteric potentiating ligand of nAChR) significantly enhanced microglial Aβ phagocytosis, and that administration of galantamine to APPswe/PS1dE9 (APdE9) transgenic mice enhanced Aβ clearance and improved behavioral performance in spatial learning and memory [20]. Furthermore, we also reported that stimulation of α7 nAChRs in a rat model of Parkinson's disease induced a direct neuroprotective effect and an indirect suppressive effect in activated microglia [21]. Nevertheless, how α7 nAChRs expressed in microglia are affected in AD remains unknown.

Recently, several studies using transgenic animal models of AD suggest that therapeutic interventions given earlier in the course of AD may be expected to improve therapeutic effects [22–25]. Therefore, prophylactic interventions in the "presymptomatic" or "preclinical" stages of AD are advocated. It has been suggested that the pathophysiological process of AD precedes the appearance of clinical symptoms in sporadic AD patients [26]. However, we found no report that describes the target and the therapeutic time window of AD treatment based on detailed analyses of the temporal profile of AD pathology and associated changes in brain environment.

Thus, we focus on microglia that are known to respond to AD pathology and are suggested to contribute to clearance of Aβ. In the present study, we hypothesized that CD68 (alias 'ED1', a member of the lysosomal/endosomal-associated membrane glycoprotein family and a marker of phagocyte in microglia/macrophage [27–30]) and α7 nAChR expression in microglia change in response to AD-like pathology. To prove this hypothesis, we used immunohistochemical studies to evaluate the temporal changes of CD68 and α7 nAChRs expressed in microglia, as well as Aβ deposition, neurons, and presynapses in the brains of two mouse models of AD. From these evaluations, we aimed to collect fundamental data for considering whether microglia are potential target of AD treatment and the appropriate timing of therapeutic intervention.

MATERIALS AND METHODS

Animals

All the animal studies were approved by the Animal Care and Use Committee of Sapporo Medical University, and all procedures were carried out in accordance with the institutional guidelines. Male and female APdE9 mice and wild-type littermates were used in this study. The APdE9 founder mice were purchased from the Jackson Laboratory, USA. All mice used in this study were bred by mating male APdE9 mice with female C57BL6/J mice in the animal facilities at Sapporo Medical University. The mice were maintained at 25°C with a 12-h light/dark cycle and provided food and water ad libitum.

The Aβ-injected AD mouse model was generated according to a previously described protocol [31, 32]. Fifteen to 30 week-old C57BL6/J mice were anesthetized intraperitoneally with 50 mg/kg pentobarbital sodium, and were immobilized in a stereotaxic frame. In this study, we used the hydrochloride (HCl) form of human $A\beta_{42}$ (AnaSpec, San Jose, CA), which aggregates more readily than $A\beta_{40}$. Additionally, the HCl form of Aβ peptide is known to form a β-sheet structure [33]. Lyophilized human $A\beta_{42}$ peptide (1 mM) was dissolved in sterile saline solution, and aliquots were stored at −80°C. Subsequently, $A\beta_{42}$ was diluted with sterile saline solution to 1 μg/μL, and then injected immediately into the left hippocampus (2 mm posterior to the bregma, 2 mm left lateral to the midline, and 2 mm ventral to the brain surface) using a motor-driven 10-μL Hamilton syringe. The infusion rate was 1 μL/min, and the needle was retained for a further 5 min after injection. Additionally, we also injected 10 mM phosphate-buffered saline (PBS) into the left hippocampus of the other C57BL6/J mice instead of $A\beta_{42}$ in such a way as described above. We defined those PBS-injected mice as controls. The volume of the injection was 1 μL of $A\beta_{42}$ or 1 μL of PBS.

For details about APdE9 mice, refer to the web site of Jackson Laboratory [strain B6.Cg-Tg (APPswe, PSEN1dE9) 85Dbo/J; stock number 005864; http://jaxmice.jax.org/]. These hemizygous APdE9 mice express chimeric mouse/human amyloid precursor protein APPswe (mouse APP695 harboring a human Aβ domain with mutations K595 N and M596 L linked to Swedish familial AD pedigrees) and human mutated presenilin 1-dE9 (deletion of exon 9). These mutations are associated with early-onset AD, and allow the mice to secrete human Aβ.

Brain tissue preparation

At 1, 3, 7, 14, and 28 days after Aβ or PBS injection, Aβ–injected mice ($n=4$ per group at each time point) and PBS-injected mice ($n=4$ per group at 1,3 and 7 days after, $n=3$ per group at 14 and 28 days after) were deeply anesthetized by intraperitoneal injection of pentobarbital sodium (50 mg/kg), and perfused through the aorta with 150 mL of 10 mM PBS, followed by 150 mL of a cold fixative consisting of 4% paraformaldehyde in 100 mM phosphate buffer. After perfusion, the brain was quickly removed and postfixed for 2 days in 4% paraformaldehyde. Subsequently, the brain was transferred to 10% sucrose followed by 20% sucrose in 10 mM PBS at 4°C for immunohistochemical and histological analysis.

Three, 6, 9, 12, and 18 month-old APdE9 mice and 3, 6, 9, and 12 month-old wild-type littermates ($n=5$ per group at each time point) were deeply anesthetized by intraperitoneal injection of pentobarbital sodium (50 mg/kg). Then, the brain was quickly removed and hemisected in the midsagittal plane. One hemisphere was frozen in liquid nitrogen after dissecting the cerebellum, and stored at −80°C to be used for biochemical measurements. The other hemisphere was postfixed for 2 days in 4 % paraformaldehyde, and subsequently transferred to 10% sucrose followed by 20% sucrose in 10 mM PBS at 4°C for immunohistochemical and histological analysis.

Immunohistochemistry

The brains of Aβ- or PBS-injected C57BL6/J mice or the hemi-brains of APdE9 mice and littermates were cut into 20-μm thick slices using a cryostat, and collected in 10 mM PBS containing 0.1% sodium azide at 4°C. For each Aβ-injected mouse, eight free floating brain sections at intervals of 200 μm were picked up and incubated with mouse monoclonal antibody to Aβ (1:5,000; clone 6E10, Covance, Princeton, NJ, USA) for 3 days at 4°C. For each APdE9 mouse or wild-type littermate, four free floating brain sections containing the hippocampus at intervals of 400 μm were picked up and incubated with the following primary antibodies: mouse monoclonal anti-Aβ antibody (1:5,000), rabbit polyclonal anti-ionized calcium binding adaptor molecule 1 (Iba1) antibody (1:5,000; Wako Chemical, Osaka, Japan) for microglia, and mouse monoclonal anti-synaptophysin antibody (1:1,000; Sigma-Aldrich, St. Louis, MO, USA) for presynapses, for 3 days at 4°C. After several washes with 10 mM PBS containing 0.3% Triton X-100 (PBS-T), sections were incubated appropriately with biotinylated anti-mouse or anti-rabbit immunoglobulin (Ig)G antibody (1:2,000; Vector Laboratories, Burlingame, CA, USA) for 2 h at room temperature. The sections were then incubated with avidin peroxidase (1:4,000; ABC Elite Kit, Vector Laboratories, Burlingame, CA, USA) for 1 h at room temperature. All the sections were washed several times with PBS-T between each incubation, and labeling was visualized by incubating with 3,3'-diaminobenzidine (DAB) and nickel ammonium, which yielded a dark blue color [32]. We observed the immunostained sections of Aβ-injected mice under a light microscope, and confirmed Aβ deposition sites in the left hippocampus in each mouse. We also observed the immunostained sections of APdE9 mice and wild-type littermates under a light microscope.

Triple or double immunofluorescent staining was performed and observed under a confocal microscope. The brain sections of Aβ-injected mice were incubated with rabbit polyclonal anti-Iba1 antibody (1:5,000) and mouse monoclonal CD68 antibody (1:1,000; AbD Serotec, Raleigh, NC, USA) or microtubule-associated protein (MAP)2 antibody (1:5,000; Sigma-Aldrich, St. Louis, MO, USA) for neurons, for 3 days at 4°C. For each Aβ-injected mouse, two brain sections (containing Aβ deposition in the left hippocampus from the result of immunostaining by anti-Aβ antibody) at an interval of 200 μm were used in each immunostaining. The brain sections of PBS-injected mice were incubated with rabbit polyclonal anti-Iba1 antibody (1:5,000) and mouse monoclonal CD68 antibody (1:1,000) for 3 days at 4°C. For each PBS-injected mouse, two brain sections at an interval of 200 μm were used in each immunostaining. Furthermore, the hemi-brain sections of APdE9 mice were incubated with rabbit polyclonal anti-Iba1 antibody (1:5,000), mouse monoclonal CD68 (1:1,000) and mouse monoclonal synaptophysin (1:1,000) or mouse monoclonal α7 nAChR (1:1,000; Sigma-Aldrich, St. Louis, MO, USA) antibody for 3 days at 4°C. For

each APdE9 mouse, two brain sections at an interval of 800 μm were used in each immunostaining. Then, the sections were probed with anti-mouse IgG antibody conjugated with Alexa Fluor 488 and anti-rabbit IgG antibody conjugated with Alexa Fluor 594 (each diluted 1:2,000) for 2 h at room temperature. The brain sections of Aβ-injected and APdE9 mice were further incubated with 1-fluoro-2,5-bis(3-carboxy-4-hydroxystyryl)benzene (FSB, 1:10,000; Dojindo Laboratories, Kumamoto, Japan) for 30 min, to stain amyloid. Fluorescence was observed under a laser scanning confocal microscope (LSM510 Meta; Carl Zeiss, Jena, Germany).

Quantification of amyloid plaque burden, microglia, and presynapses of the hippocampus

In Aβ- or PBS-injected mice, multi-stained immunofluorescent images were analyzed by measuring the percentage of positively stained area in a microscopic field with ImageJ software (National Institutes of Health, Bethesda, MD, USA). Subsequently, we compared the mean percentage of FSB- or Iba1-positive area among time points. All images of the Aβ- and PBS-injected mice were acquired as TIFF images. To minimize variability of signal intensity between images, we used the same image acquisition settings (exposure time and gain) for each antibody signal throughout the assessments of Aβ- and PBS-injected mice.

In APdE9 mice and wild-type littermates, DAB-labeled sections stained by anti-Aβ and anti-Iba1 or anti-synaptophysin antibodies were analyzed by measuring the percentage of positively stained area in a microscopic field using ImageJ software (percentage of synaptophysin-positive area was measured per area of the hilus of the dentate gyrus in a microscopic field). Then, we compared the mean percentage of Aβ-, Iba1-, or synaptophysin-positive areas among age groups.

All images were binarized with the same threshold for each antibody signal using Adobe Photoshop CS6 software, and the percentage of positively stained area was measured.

Quantitative analysis of CD68- or α7 nAChR-positive microglia

The percentage of Iba1-positive microglia co-expressing CD68 per total Iba1-positive microglia was assessed in the triple-stained immunofluorescent images of Aβ- or PBS-injected mice and APdE9 mice. Subsequently, we compared the mean percentage of CD68-positive microglia among different time points. In addition, the percentage of Iba1-positive microglia co-expressing α7 nAChR subunit per total Iba1-positive microglia was assessed in the triple-stained immunofluorescent images of APdE9 mice. Then, we compared the mean percentage of α7 nAChR-positive microglia among age groups. We used the same image acquisition settings (exposure time and gain) for each immunostaining series.

Enzyme-linked immunosorbent assay (ELISA)

In order to measure the amount of $A\beta_{42}$ in the brain of APdE9 mice, a Tris-buffered saline (TBS) extracted fraction and a formic acid (FA) extracted fraction were prepared according to the following procedures as described previously [20, 34]. The frozen hemi-brain of a mouse (200 mg/ml wet weight) was suspended in TBS (20 mM Tris HCl and 137 mM NaCl, pH 7.6) containing protease inhibitors (P8340, protease inhibitor cocktail; Sigma-Aldrich, St. Louis, MO, USA) and homogenized using a high-speed homogenizer (60 s at 10,000 rpm; Polytron PT2500E; Kinematica AG, Luzern, Switzerland). The homogenate was centrifuged at 100,000× *g* for 1 h at 4°C, and the supernatant was collected as the TBS-extracted fraction. The pellet was sonicated in 70% FA. This homogenate was incubated for 1 h at 4°C, and then centrifuged at 100,000× *g* for 1 h at 4°C. The resultant supernatant was collected as the FA-extracted fraction, which was neutralized with a 20-fold volume of 1M Tris buffer (pH 11.0). The $A\beta_{42}$ in the neutralized FA-extracted fraction was measured using a human $A\beta_{42}$-specific ELISA kit (Invitrogen, Carlsbad, CA, USA) according to the manufacturer's instructions.

Statistics

The percentage of positively stained area, the percentage of microglia expressing CD68 or α7 nAChR, and the amount of $A\beta_{42}$ in the brain of model mice are presented as mean ± SEM. The differences between groups were analyzed by Student's *t*-test or ANOVA followed by *post hoc* comparison with Tukey-Kramer HSD test. The JMP statistical program (SAS Institute, Cary, NC, USA) was used for data analysis.

RESULTS

CD68-positive activated microglia phagocytosed Aβ deposition early after Aβ injection

We first examined the temporal changes of Aβ deposition by microscopic observation of immunoreactivity

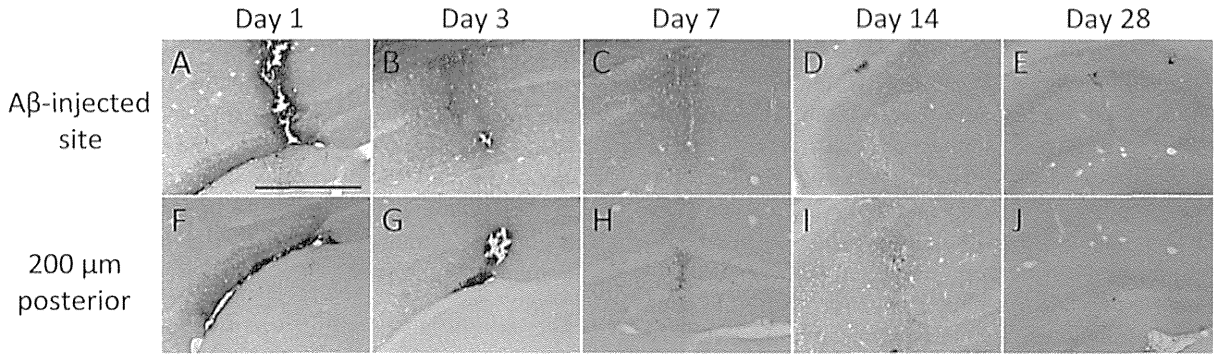

Fig. 1. Representative photomicrographs of immunoreactivity to anti-amyloid-β (Aβ) antibody at the injection site (A–E) and at 200 μm posterior to the injection site (F–J) in the hippocampus of Aβ-injected mice at various time points. Mice were microinjected with $Aβ_{42}$ into the left hippocampus, and subsequently euthanized at 1 day (A, F), 3 days (B, G), 7 days (C, H), 14 days (D, I), and 28 days (E, J) after injection. Scale bar = 500 μm in A (applies to A–I).

to anti-Aβ antibody at the injection site and at 200 μm posterior to the injection site in ipsilateral hippocampus (Fig. 1). At 1 day after intrahippocampal injection of $Aβ_{42}$, Aβ deposition was clearly detected (Fig. 1A, F). Thereafter, the Aβ deposition decreased in a time-dependent manner (Fig. 1B–E, G–J).

To analyze the relationship of Aβ deposition with microglia and neurons, we observed triple immunofluorescence staining for Iba1, FSB, and CD68 (Fig. 2A–E) and for Iba1, FSB, and MAP2 (Fig. 2F–J) in brain sections of the ipsilateral hippocampus of Aβ-injected mice, using a laser scanning confocal microscope. Additionally, double-stained immunofluorescent images for FSB and Iba1 in the ipsilateral (Fig. 2K–O) and the contralateral hippocampus (Fig. 2P–T) were assessed by measuring the percentage of positively stained area in a microscopic field, and the differences between groups were compared.

The Aβ deposition stained by FSB decreased in a time-dependent manner (Fig. 2A–T). The mean percentage of FSB-positive area assessed as Aβ burden also decreased in a time-dependent manner (Fig. 3A). Aβ deposition was not observed in the contralateral hippocampus (Fig. 2P–T).

Microglial accumulation, immunostained by anti-Iba1 antibody, at the Aβ deposition sites was already observed at 1 day after Aβ injection (Fig. 2A, F, K). In quantitative analysis, the Iba1-positive area was significantly larger (3.8-fold) on the Aβ-injected side than on the contralateral side at 1 day after Aβ injection (Fig. 3B). Then, microglial accumulation increased gradually until 7 days after Aβ injection, and subsequently decreased in a time-dependent manner (Figs. 2B–E, 2G–J, 2L–O, and 3B). In addition, several microglia showed a positive reaction with the anti-CD68 antibody from 1 day after Aβ injection, and microglia internalizing Aβ probed with FSB were observed at all time points (Fig. 2A–E). However, the percentage of Iba1-positive microglia co-expressing CD68 per total Iba1-positive microglia in a microscopic field of the Aβ-injected hippocampus was not significantly different among time points (Fig. 3C). To exclude the possibility of effect by injection injury, we examined the temporal changes of microglia in PBS-injected mice (Supplementary Figure 1). Accumulation of microglia in PBS-injected mice was more homogeneous and less than in Aβ-injected mice (Supplementary Figure 1A–J). In quantitative analysis, the Iba1-positive area increased gradually until 7 days after PBS injection and decreased subsequently in the same way as Aβ-injected mice. However, microglial accumulation in PBS-injected mice was significantly less than Aβ-injected mice at 7 and 28 days after injection (Supplementary Figure 1K), and marginally less than Aβ-injected ones at 14 days after ($p = 0.0944$). On the other hand, the percentage of Iba1-positive microglia co-expressing CD68 per total Iba1-positive microglia in a microscopic field of the PBS-injected hippocampus increased gradually until 7 days after PBS injection, and decreased significantly from 14 days after (Supplementary Figure 1L). These results in PBS-injected mice are obviously different from Aβ-injected ones. Therefore, these findings suggest that the histochemical results in Aβ-injected mice were produced by not needle insertion injury but Aβ injection.

We confirmed that activated microglia phagocytosed Aβ deposit in Aβ-injected mice based on

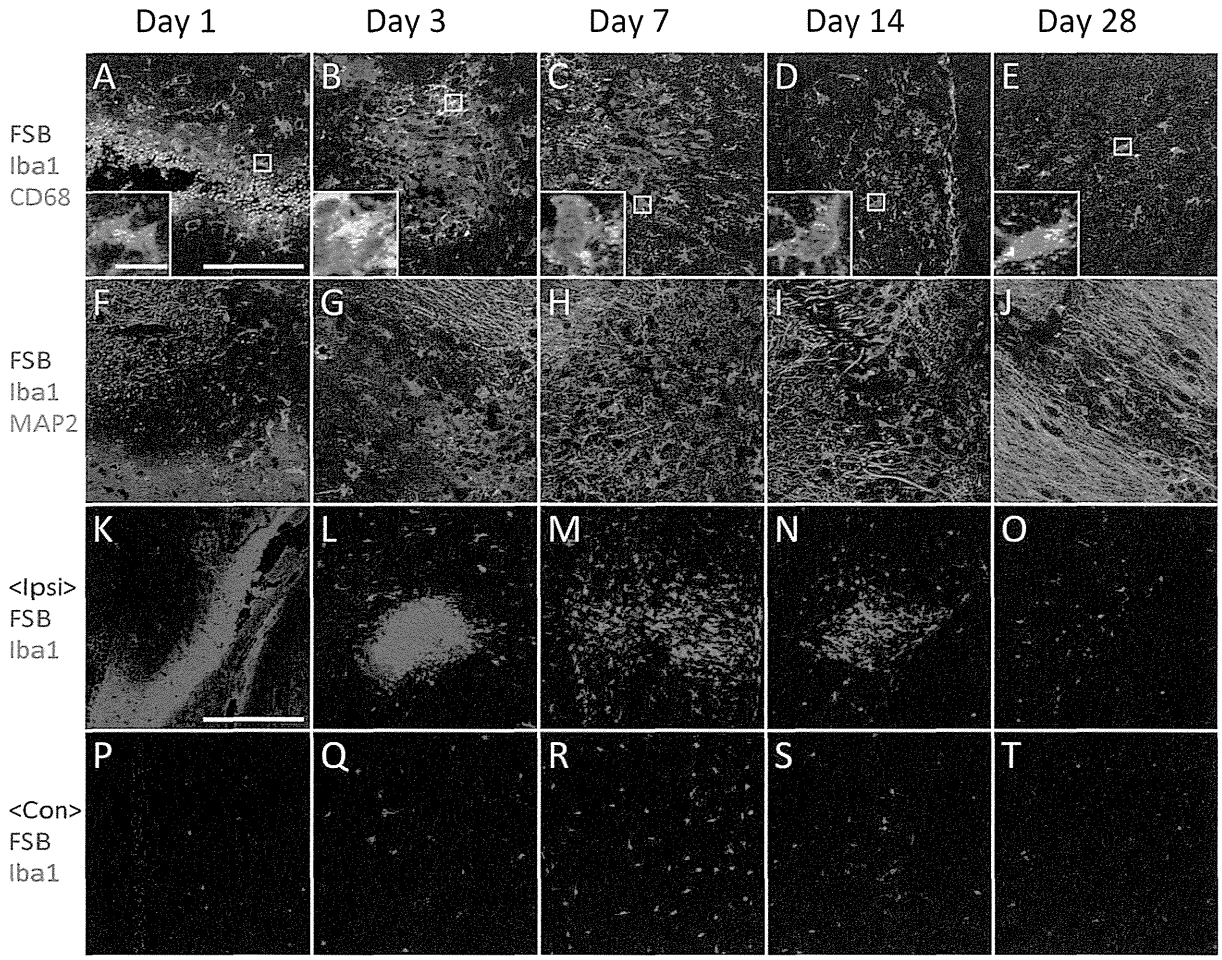

Fig. 2. Triple-staining immunofluorescent images for FSB (*blue*), Iba1 (*red*), and CD68 (*green*; A–E), as well as FSB (*blue*), Iba1 (*red*), and MAP2 (*green*; F–J) at the hippocampus of amyloid-β (Aβ)-injected mice at 1 day (A, F, K, P), 3 days (B, G, L, Q), 7 days (C, H, M, R), 14 days (D, I, N, S), and 28 days (E, J, O, T) after injection. K–T) Time courses of Aβ and microglial activation at the ipsilateral (K–O) and at the contralateral hippocampus (P–T) of Aβ-injected mice. Seven or 8 double-staining immunofluorescent images for FSB (*blue*) and Iba1 (*red*) were assessed in each mouse. Scale bars = 100 μm in A (applies to A–J); 10 μm in insets; 200 μm in K (applies to K–T). FSB, 1-fluoro-2,5-bis(3-carboxy-4-hydroxystyryl)benzene; Iba1, ionized calcium binding adaptor molecule 1; MAP2, microtubule-associated protein 2; Ipsi, ipsilateral; Con, contralateral.

the following evidence: (1) microglia were closely associated with Aβ deposits (Fig. 2) and internalized Aβ as in our previous *in vitro* study [8] (Fig. 2A–E); (2) microglia expressed CD68 which is a phagocytic marker (Fig. 2A–E); (3) Aβ deposition decreased markedly coinciding with a drastic increase in microglial accumulation until 7 days after Aβ injection, followed by disappearance of Aβ deposition as microglia accumulation decreased gradually.

The MAP2-immunoreactive area decreased at 1 day after Aβ injection (Fig. 2F), but subsequently recovered in a time-dependent manner (Fig. 2G–J). The neurotoxicity of acute Aβ-injection may not be potent.

In APdE9 mice, Aβ deposition estimated immunohistochemically increased gradually and correlated strongly with mean quantity of insoluble $A\beta_{42}$ measured by ELISA

In APdE9 mice, photomicroscopic images of Aβ immunostaining were assessed by measuring the percentage of positively stained area in a high power microscopic field of the cortex and hippocampus (Fig. 4A–E, areas surrounded by grey squares). The Aβ burden increased in a time-dependent manner, with a drastic increase at 12 months of age (Fig. 5A). In a similar quantitative analysis in wild-type littermates at

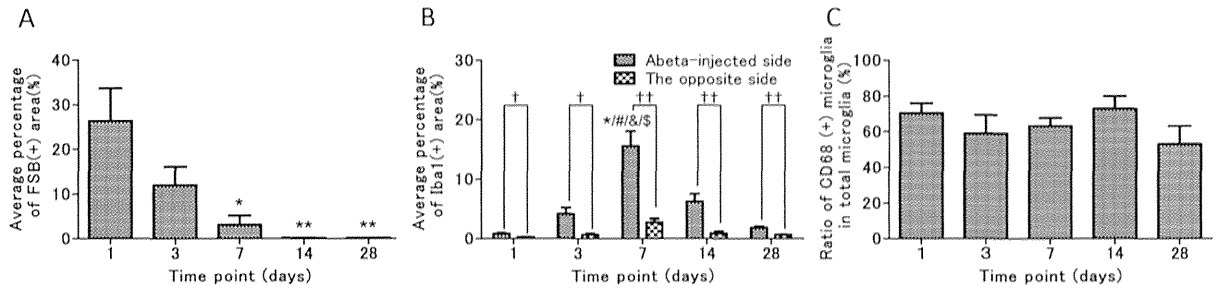

Fig. 3. Quantitative analyses of amyloid plaque burden, Iba1-positive area, and CD68-positive microglia in amyloid-β (Aβ)-injected mice. Data are presented as the percentage of positively stained area in a microscopic field, and expressed as mean ± SEM at each time point ($n=4$). A) Time course of Aβ burden assessed as FSB-positive area in ipsilateral hippocampus measured using ImageJ software. The mean percentages of FSB-positive area at different time points were compared by ANOVA [$F(4,15)=8.2982$, $p=0.0010$] followed by *post hoc* Tukey-Kramer HSD test: $^{*}p<0.01$, $^{**}p<0.005$ versus 1 day after injection. B) Time course of microglial activation assessed as Iba1-positive area in bilateral hippocampi measured using ImageJ software. The mean percentages of Iba1-positive area on the Aβ-injected side at different time points were compared by ANOVA [$F(4,15)=18.4849$, $p<0.0001$] followed by *post hoc* Tukey-Kramer HSD test: $^{*}p<0.001$ versus 1 day, $^{\#}p<0.0005$ versus 3 days, $^{\&}p<0.05$ versus 14 days, and $^{\$}p<0.0001$ versus 28 days after injection. The mean percentages of Iba1-positive area on the Aβ-injected side and the contralateral side were compared by Student's *t*-test: $^{\dagger}p<0.01$, $^{\dagger\dagger}p<0.005$. C) Time course of percentage of CD68-positive microglia per total microglia in ipsilateral hippocampus. The mean percentages of Iba1-positive microglia co-expressing CD68 per total Iba1-positive microglia at different time points were compared by ANOVA [$F(4,15)=1.0747$, $p=0.4035$]. FSB, 1-fluoro2,5-bis (3-carboxy-4-hydroxystyryl) benzene; Iba1, ionized calcium binding adaptor molecule 1.

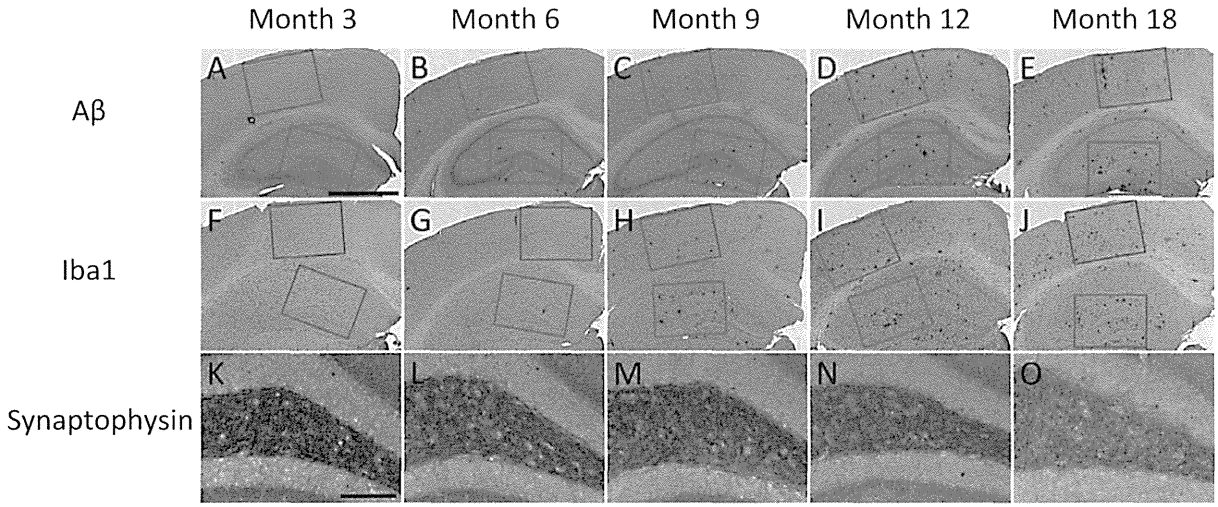

Fig. 4. Representative photomicrographs of amyloid-β (Aβ) immunoreactivity (A–E), Iba1-immunopositive microglia (F–J), and synaptophysin immunoreactivity (K–O) in the hilus of the dentate gyrus in APPswe/PS1dE9 (APdE9) mice. Sections of the hemi-brain from mice at 3 months (A, F, K), 6 months (B, G, L), 9 months (C, H, M), 12 months (D, I, N), and 18 months (E, J, O) of age were stained with each primary antibody. Scale bars = 1 mm in A (applies to A–J); 100 μm in K (applies to K–O). Iba1, ionized calcium binding adaptor molecule 1.

3, 6, 9, and 12 months of age, the mean percentage of Aβ-positive area was almost 0%, and there was no significant difference compared with APdE9 mice at 3 months of age (data not shown).

Subsequently, to verify the validity of evaluating Aβ-positive area in immunohistochemical study, we measured the quantity of human $Aβ_{42}$ in neutralized FA-extracted fraction from the cerebral hemisphere of APdE9 mice, using a human $Aβ_{42}$-specific ELISA kit (Fig. 5B). Pearson's correlation coefficient showed a significant correlation between the mean quantity of $Aβ_{42}$ for each time point measured by ELISA and the mean percentage of Aβ-positive area for each time point estimated immunohistochemically (Fig. 5C). Therefore, the method of measuring mean percentage of the Aβ-immunopositive area at each time point

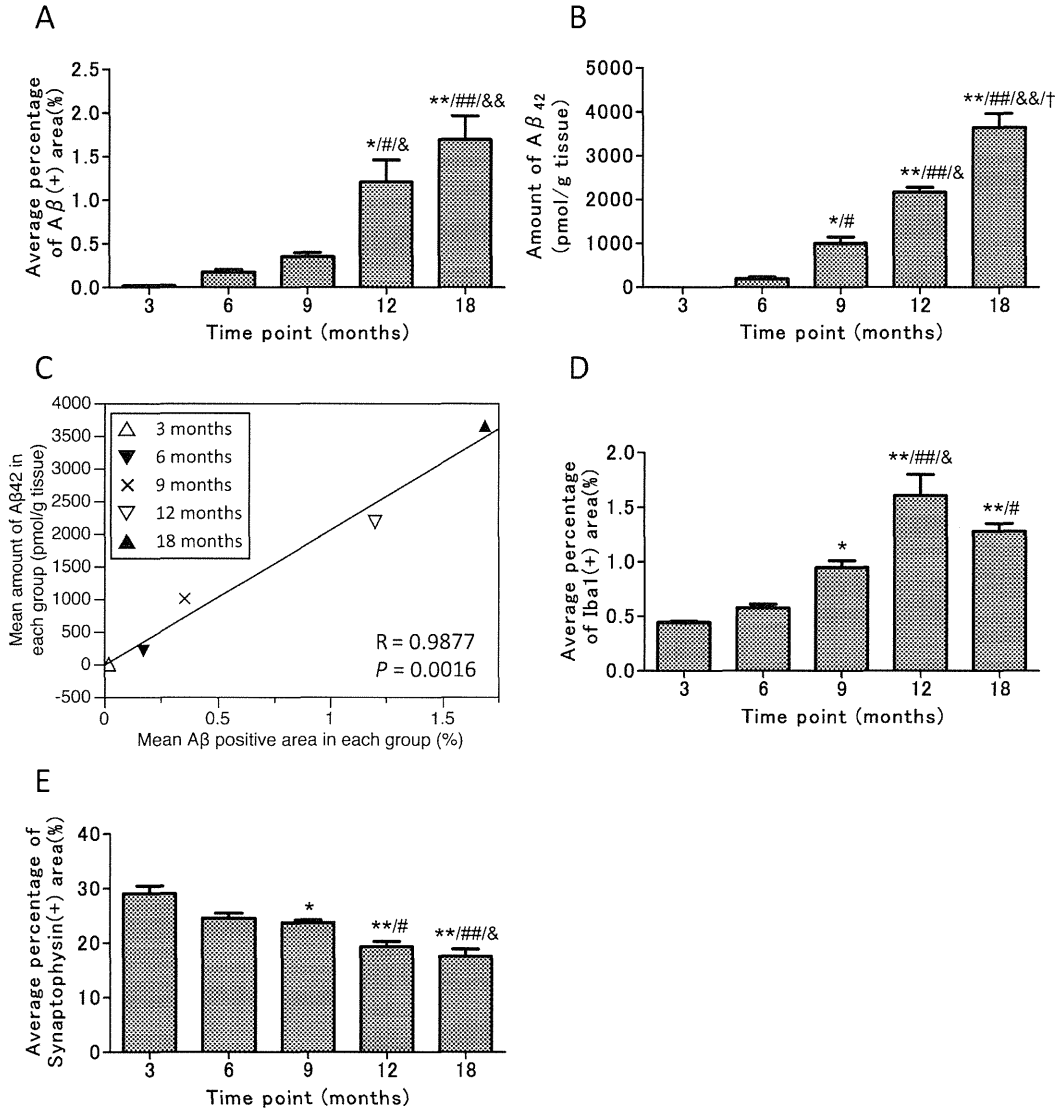

Fig. 5. Quantitative analysis of amyloid plaque burden, Iba1-positive area and synaptophysin-positive area, and amount of $A\beta_{42}$ in the cerebral hemisphere measured by ELISA, in APdE9 mice. Aβ burden was assessed as Aβ-positive areas in the cortex and hippocampus of 4 sections/animal measured using ImageJ software. A) The mean percentages of Aβ-positive area in a high power microscopic field of the cortex and hippocampus (areas enclosed by grey squares in Fig. 4A–E) in different age groups were compared by ANOVA [$F(4,20)=18.7716$, $p<0.0001$] followed by *post hoc* Tukey-Kramer HSD test: $^{*}p<0.001$, $^{**}p<0.0001$ versus 3 month-old group, $^{\#}p<0.005$, $^{\#\#}p<0.0001$ versus 6 month-old group, $^{\&}p<0.05$, $^{\&\&}p=0.0001$ versus 9 month-old group. B) The mean quantities of $A\beta_{42}$ in the cerebral hemisphere of APdE9 mice measured by ELISA at different age groups were compared by ANOVA [$F(4,20)=84.0981$, $p<0.0001$] followed by *post hoc* Tukey-Kramer HSD test: $^{*}p<0.005$, $^{**}p<0.0001$ versus 3 month-old group, $^{\#}p<0.05$, $^{\#\#}p<0.0001$ versus 6 month-old group, $^{\&}p<0.001$, $^{\&\&}p<0.0001$ versus 9 month-old group, $^{\dagger}p<0.0001$ versus 12 month-old group. C) The mean percentage of Aβ-positive area for each age group assessed immunohistochemically correlates strongly with mean quantity of $A\beta_{42}$ for each age group measured by ELISA. Correlation was tested using the Pearson's correlation coefficient. Microglial activation was assessed as Iba1-positive areas in the cortex and hippocampus of 4 sections/animal measured using ImageJ software. D) The mean percentages of Iba1-positive area in a high power microscopic field of the cortex and hippocampus (areas enclosed by grey squares in Fig. 4F–J) in different age groups were compared by ANOVA [$F(4,20)=24.4838$, $p<0.0001$] followed by *post hoc* Tukey-Kramer HSD test: $^{*}p<0.05$, $^{**}p<0.0001$ versus 3 month-old group, $^{\#}p=0.0005$, $^{\#\#}p<0.0001$ versus 6 month-old group, $^{\&}p<0.001$ versus 9 month-old group. E) Density of presynapses was assessed as synaptophysin-positive area at the hilus of the dentate gyrus of 4 sections/animal measured using ImageJ software. The mean percentages of synaptophysin-positive area in a high power microscopic field in different age groups were compared by ANOVA [$F(4,20)=17.9074$, $p<0.0001$] followed by *post hoc* Tukey-Kramer HSD test: $^{*}p<0.05$, $^{**}p<0.0001$ versus 3 month-old group, $^{\#}p<0.05$, $^{\#\#}p<0.005$ versus 6 month-old group, $^{\&}p<0.01$ versus 9 month-old group. Iba1, ionized calcium binding adaptor molecule 1.

was considered to be appropriate for assessing Aβ burden.

In APdE9 mice, microglial accumulation was closely associated with the Aβ plaques; but some activated microglia were found at sites without Aβ deposition, especially at an early age

In APdE9 mice, microglia labeled by anti-Iba1 antibody were closely associated with Aβ deposits, and their accumulation increased in a time-dependent manner until 12 months of age (Fig. 6A–J). On the other hand, some swollen microglia considered to be activated were also found at sites where there was no Aβ deposition, especially at 6 or 9 months of age (Fig. 6B, C, G, H). We assessed the photomicroscopic images of Iba1 immunostaining by measuring the percentage of positively stained area in a high power microscopic field of the cortex and hippocampus (Fig. 4F–J, areas surrounded by grey squares). Microglia increased significantly at 9 months and further increased at 12 months of age (Fig. 5D). On the other hand, Iba1-positive area declined at 18 months of age compared to 12 months of age.

In APdE9 mice, immunoreactivity for presynapses at the hilus of dentate gyrus decreased homogeneously in a time-dependent manner since an early age

We observed triple-immunofluorescence staining for Iba1, FSB, and synaptophysin at the hilus of the dentate gyrus in the hippocampus (Fig. 6K–O) of APdE9 mice. Photomicroscopic images of synaptophysin immunostaining (Fig. 4K–O) were assessed by measuring the percentage of positively stained area at the hilus of the dentate gyrus. The density of presynapses decreased in a time-dependent manner (Figs. 4K–O, 6K–O). In quantitative analysis, the density of presynapses decreased significantly at 9, 12, and 18 months of age (Fig. 5E). The decrease in presynapse immunoreactivity was homogeneous and not confined to the Aβ deposition sites. In addition, Student's *t*-test detected a significantly lower mean percentage of synaptophysin-positive area in APdE9 mice compared to age-matched wild-type littermates from 3 to 12 months of age (Supplementary Figure 2). We speculate that normal aging causes the decrease of the synaptophysin level in wild-type littermates at 12 months of age.

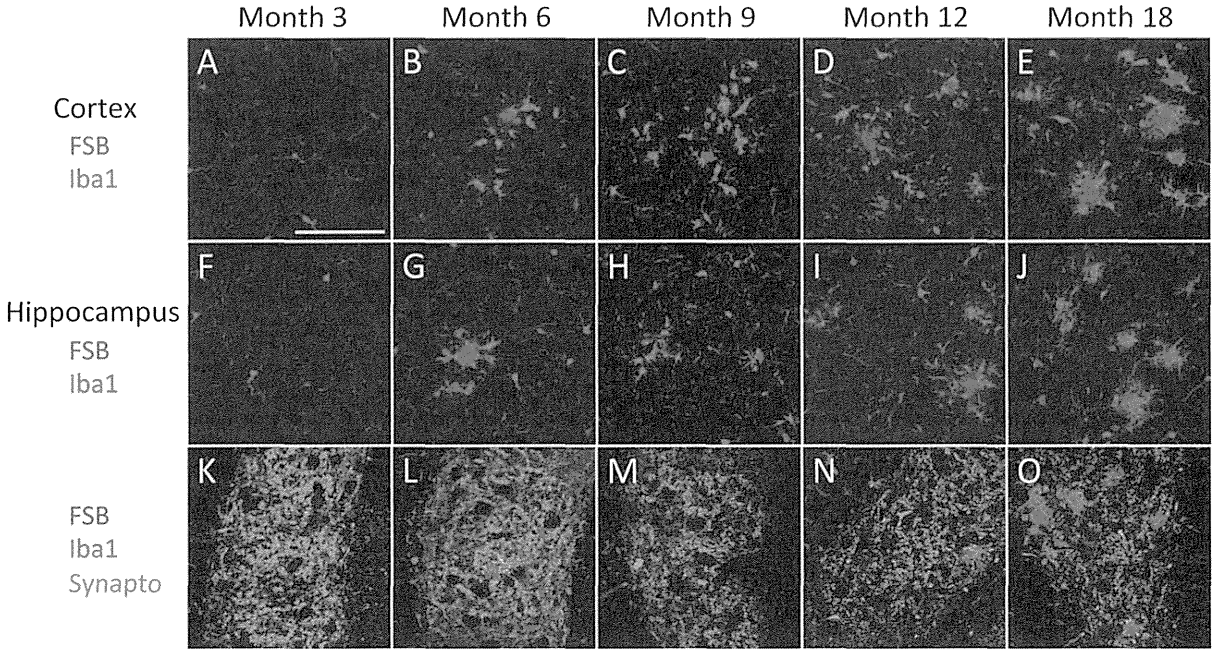

Fig. 6. Double-staining immunofluorescent images for FSB (*blue*) and Iba1 (*red*) at the cortex (A–E) and hippocampus (F–J), and triple-staining immunofluorescent images for FSB, Iba1, and synaptophysin (*green*; K–O) at the dentate gyrus of hippocampus in APPswe/PS1dE9 (APdE9) mice. The brain sections were from mice aged 3 months (A, F, K), 6 months (B, G, L), 9 months (C, H, M), 12 months (D, I, N), and 18 months (E, J, O). Scale bar = 100 μm in A (applies to A-O). FSB, 1-fluoro-2,5-bis (3-carboxy-4-hydroxystyryl) benzene; Iba1, ionized calcium binding adaptor molecule 1; Synapto, synaptophysin.

Percentage of CD68-positive microglia per total Iba1-positive microglia increased drastically at 12 months of age corresponding to increase in Aβ deposition in APdE9 mice

To analyze temporal changes of microglial activity in APdE9 mice, percentage of Iba1-positive microglia co-expressing CD68 per total Iba1-positive microglia in a microscopic field of the cortex and hippocampus in the triple-staining immunofluorescent images for FSB, Iba1, and CD68 was assessed in each age group (Fig. 7A–E; higher magnification Fig. 7F–J). CD68-positive microglia were not found at 3 months of age, but a small number appeared at 6 and 9 months of age. The mean percentage of Iba1-positive microglia co-expressing CD68 per total Iba1-positive microglia increased drastically at 12 months of age (Fig. 9A). This timing seemed to coincide with the increase in Aβ deposition in APdE9 mice. The mean percentage of Iba1-positive microglia co-expressing CD68 decreased at 18 months of age compared to 12 months of age. Higher magnification images (Fig. 7*a–t*) showed that CD68-negative swollen microglia, considered to be activated microglia, were also found in sites where there was no Aβ deposition, and these microglia internalized small FSB-positive structures resembling small Aβ, especially at 6 or 9 months of age (Fig. 7*e–l*). These microglia were speculated to take up soluble Aβ because there was no Aβ deposit around them. On the other hand, CD68-positive, more swollen microglia took up larger FSB-positive Aβ deposits (Fig. 7*m–t*).

Percentage of α7 nAChR-positive microglia per total Iba1-positive microglia increased drastically at 6 months of age, and thereafter decreased in a time-dependent manner in APdE9 mice

Percentage of Iba1-positive microglia co-expressing α7 nAChR per total Iba1-positive microglia in a microscopic field of the cortex and hippocampus in the triple-

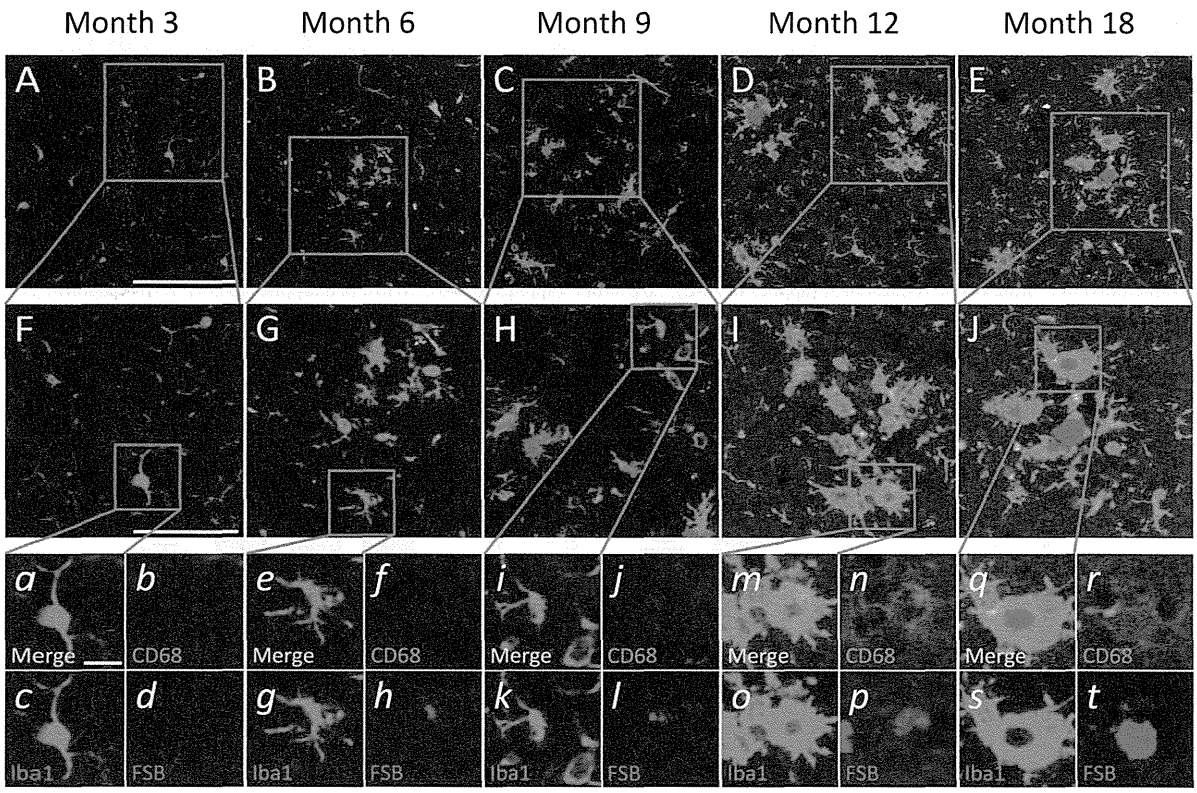

Fig. 7. Triple-staining immunofluorescent images for FSB (*blue*), Iba1 (*red*), and CD68 (*green*) in APPswe/PS1dE9 (APdE9) mice at various ages. Triple immunofluorescence staining with FSB, anti-Iba1 antibody, and anti-CD68 antibody were performed on sections of the hemi-brain collected from mice aged 3 months (A, F, *a–d*), 6 months (B, G, *e–h*), 9 months (C, H, *i–l*), 12 months (D, I, *m–p*), and 18 months (E, J, *q–t*). Areas enclosed by red squares in A to E are magnified in F to J, respectively. Areas enclosed by red squares in F to J are magnified in *a* to *t*. In G, *e–h* and H, *i–l*, microglia are CD68-negative and located apart from Aβ deposition sites. These microglia internalize very small amount of Aβ stained blue by FSB. Scale bars = 100 μm in A (applies to A–E); 50 μm in F (applies to F–J); 10 μm in *a* (applies to *a–t*). FSB, 1-fluoro-2,5-bis (3-carboxy-4-hydroxystyryl) benzene; Iba1, ionized calcium binding adaptor molecule 1.

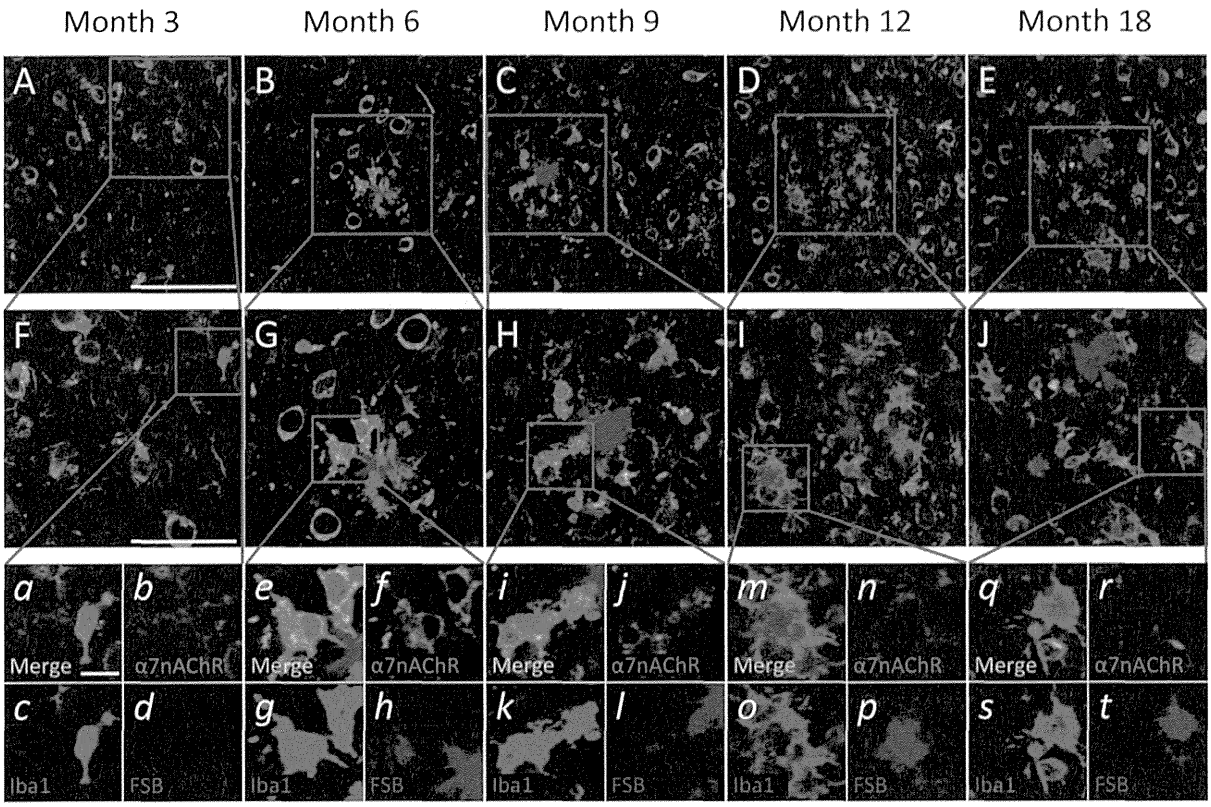

Fig. 8. Triple-staining immunofluorescent images for FSB (*blue*), Iba1 (*red*), and α7 nAChR (*green*) in APPswe/PS1dE9 (APdE9) mice at various ages. Triple immunofluorescence staining with FSB, anti-Iba1 antibody and anti-α7 nAChR antibody was performed on sections of the cerebral hemisphere collected from mice aged 3 months (A, F, *a–d*), 6 months (B, G, *e–h*), 9 months (C, H, *i–l*), 12 months (D, I, *m–p*), and 18 months (E, J, *q–t*). Area enclosed by red squares in A to E are magnified in F to J, respectively. Areas enclosed by red squares in F to J are magnified in *a* to *t*. Scale bars = 100 μm in A (applies to A–E); 50 μm in F (applies to F–J); 10 μm in *a* (applies to *a–t*). FSB, 1-fluoro-2,5-bis (3-carboxy-4-hydroxystyryl) benzene; Iba1, ionized calcium binding adaptor molecule 1; α7 nAChR, α7 nicotinic acetylcholine receptor.

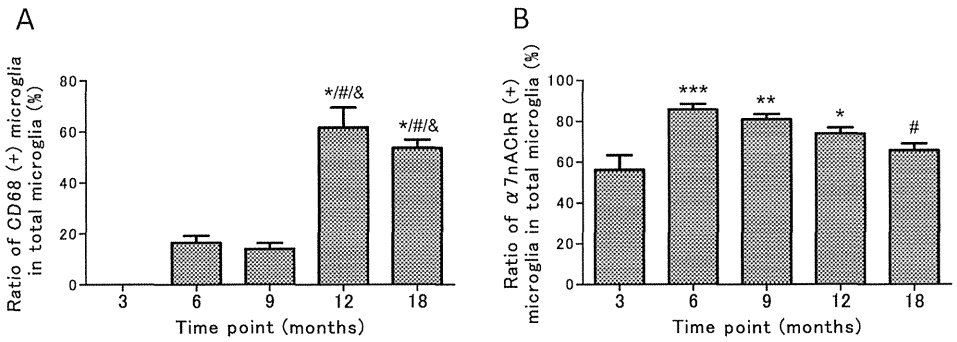

Fig. 9. Percentage of CD68-positive microglia and percentage of α7 nAChR-positive microglia per total microglia in a microscopic field of the cortex and hippocampus of APPswe/PS1dE9 (APdE9) mice at various ages. Data were expressed as mean ± SEM of each age group ($n = 5$). A) The mean percentages of CD68-positive microglia at different age groups were compared by ANOVA [$F(4,20)=42.8589$, $p < 0.0001$] followed by *post hoc* Tukey-Kramer HSD test: $^{*}p < 0.0001$ versus 3 month-old group, $^{\#}p < 0.0001$ versus 6 month-old group, $^{\&}p < 0.0001$ versus 9 month-old group. B) The mean percentages of α7 nAChR-positive microglia in different age groups were compared by ANOVA [$F(4,20) = 8.2952$, $p = 0.0004$] followed by *post hoc* Tukey-Kramer HSD test: $^{*}p < 0.05$, $^{**}p < 0.005$, $^{***}p = 0.0005$ versus 3 month-old group, $^{\#}p < 0.05$ versus 6 month-old group. α7 nAChR, α7 nicotinic acetylcholine receptor.

staining immunofluorescent images for FSB, Iba1, and α7 nAChR was assessed at each time point (Fig. 8A–E; higher magnifications Fig. 8F–J). The mean percentage of Iba1-positive microglia co-expressing α7 nAChR per total Iba1-positive microglia increased significantly at 6 months of age (Fig. 9B). This timing seemed to coincide with the time when Aβ began to deposit and activated microglia appeared for the first time. Thereafter, the mean percentage of α7 nAChR-positive microglia decreased in a time-dependent manner coinciding with the increase in Aβ deposition (Fig. 9B). Higher magnification images (Fig. 8*a–t*) showed that α7 nAChR in microglia expressed more strongly at 6 or 9 months of age than other times (Fig. 8*e–l*).

DISCUSSION

In the present study, we hypothesized that microglial activation and expression of α7 nAChR in microglia change in response to AD-like pathology in animal models of AD. Thus, we observed the pathological changes in the brains of animal models of AD.

We first produced an AD mouse model by injecting $A\beta_{42}$ into the left hippocampus, and observed the temporal changes of Aβ deposition, microglia, and neurons. CD68 is known as a phagocytic marker of microglia/macrophage [27–30]. We confirmed that CD68-positive microglia phagocytosed Aβ deposits based on their close association with Aβ deposits as well as the temporal changes of Aβ and microglia. In a previous study using Aβ-injected rats similar to our mouse model, electron microscopic observation revealed that the Aβ deposits contained large numbers of fibrils [35]. Therefore, we speculate that the Aβ deposition in our Aβ-injected mice is mainly composed of fibrillar Aβ. Early microglial accumulation closely associated with Aβ deposition was consistent with previous reports [2, 8]. However, no report has described temporal changes of CD68-positive microglia in the Aβ-injected mouse model. Findings in this model suggest that acute Aβ deposition may induce resting microglia to transform to CD68-positive microglia within a short period of time, and that the CD68-positive microglia may contribute to clearance of Aβ deposits composed mainly of fibrillar Aβ.

In the immunohistochemical evaluation of APdE9 mice, we observed gradual increase in Aβ deposition concurrent with microglial accumulation at the sites of Aβ deposition from 6 to 12 months of age. These results are similar to previous reports [36, 37]. In APdE9 mice, activated microglia were also confirmed to take up Aβ, because of their close association with Aβ deposits. Moreover, activated microglia in APdE9 mice showed two-step transition: CD68-negative microglia appeared at 6–9 months of age, and strongly CD68-positive microglia appeared from 12 months of age. The results obtained in APdE9 mice differ markedly from those observed in the Aβ-injected mice in which CD68-positive microglia accumulated at the Aβ deposition sites in the early stage.

A review describes the CD68-positive and CD68-negative forms of activated microglia [38]. Previous reports have shown that CD68 immunoreactivity disappears completely in fully differentiated resting microglia of postnatal rat brains [39] and that resting microglia can become CD68-positive cells following CNS injury [40]. Additionally, CD68 antigen is expressed rapidly on microglia following acute traumatic injuries, but few activated microglia that accumulate in the facial nucleus after an axotomy express CD68 antigen [41]. Hence, it is possible that there exist many different microglial activation states, which are determined largely by the specific nature of the CNS lesion or disturbance. However, our search of literature found no report on the temporal changes of CD68 expression in activated microglia in the brain of AD transgenic mice. In this regard, our results have important novelty. Based on the results obtained in this study, the two-step transition of activated microglia with respect to CD68 expression in APdE9 mice will be discussed.

In APdE9 mice used in the present study, CD68-negative microglia also internalized small FSB-positive Aβ at 6 or 9 months of age (Fig. 7*e–l*). These CD68-negative microglia probably internalized soluble Aβ rather than the fibrillar Aβ, because there was no Aβ deposition around the CD68-negative microglia harboring small Aβ. Furthermore, a previous report has described the detection of Aβ oligomers by 1-bromo-2,5-bis(3-hydroxycarbonyl-4-hydroxy)styrylbenzene (BSB), which is the bromine analog of FSB and has almost the same properties as FSB [42]. On the other hand, the percentage of CD68-positive microglia increased markedly from 12 months of age when Aβ deposits also increased in APdE9 mice, and was consistently high in the brains of Aβ-injected mice in which large quantities of Aβ deposited from 1 day after Aβ injection. Accordingly, increase in Aβ deposition accompanying progression of AD-like pathology in APdE9 mice seems to be the factor triggering the activation of microglia from CD68-negative to CD68-positive form, and CD68-positive activated microglia in older APdE9 mice may contribute to clearance of Aβ deposits as in the Aβ-injected mice. These findings suggest that CD68-negative activated

microglia may contribute to the clearance of soluble Aβ in younger APdE9 mice, while CD68-positive activated microglia may participate in the clearance of Aβ deposits composed mainly of fibrillar Aβ in Aβ-injected mice and older APdE9 mice.

Incidentally, accumulation of microglia decreased at 18 months of age in APdE9 mice. Several previous reports have shown that an increase of Aβ deposition induces microglial dysfunction [43, 44]. Therefore, the tendency of decreasing microglial activity in older APdE9 mice may also be caused by the increase of Aβ deposition.

In the present study, decrease of presynapses in the brains of APdE9 mice was homogeneously and not confined to Aβ deposition sites. This result suggests that the early decrease of presynapses in APdE9 mice may be caused by soluble Aβ rather than Aβ deposits. Recently, soluble Aβ oligomers have been suggested to cause synaptic dysfunction and cell death in AD pathology [45–47]. Therefore, inducing microglia to the CD68-negative activated form may be a promising therapeutic strategy for AD. Different from the mechanism of phagocytosis of fibrillar Aβ by microglia, several theories have been proposed on how microglia internalize soluble Aβ, such as phagocytosis mediated by class A1 scavenger receptors (*Scara1*) [48] and macropinocytosis [49]. The difference in mechanisms of taking up soluble and fibrillar Aβ may be due to the different forms of microglia involved.

To the best of our knowledge, there are few reports suggesting that microglia show two-step transition in transgenic mouse models of AD. Therefore, the results of detailed temporal observation in the present study are important to analyze the pathology of AD, develop new therapeutic theory for AD, and discuss the optimal timing for therapeutic intervention against AD.

The mean percentage of α7 nAChR-positive microglia increased drastically at 6 months of age when Aβ began to deposit and Iba1-positive microglia co-expressing CD68 appeared for the first time. These findings suggest that α7 nAChR expressed in microglia may play a role in modulating microglial activation in the transgenic mouse model of AD. Previous studies report that α7 nAChR stimulation or upregulation of α7 nAChR expression in microglia reduces the production of proinflammatory cytokines such as TNFα by microglia [18, 50–52]. It would be interesting to hypothesize that α7 nAChR expressed in microglia is related to the induction of CD68-negative activated microglia and anti-inflammatory effects. The findings of the present study may suggest a potential new therapeutic strategy against AD by targeting α7 nAChR expressed in microglia, which transforms resting microglia to CD68-negative activated microglia that have neuroprotective and anti-inflammatory effects and increase Aβ clearance. After the marked increase at 6 months of age, the mean percentage of α7 nAChR-positive microglia decreased thereafter in a time-dependent manner, as Aβ deposition continued to increase. The gradual decline in percentage of α7 nAChR-positive microglia correlating negatively with the gradual increase in Aβ deposition may support previous reports that increased Aβ deposition induces dysfunction of microglia [43, 44].

To prove that the increase in CD68-positive microglia or α7 nAChR-positive microglia is associated with Aβ, it is necessary to confirm the different α7 nAChR effects in various pathophysiological stages; for example, how stimulation of the α7 nAChR affects CD68-positive microglia in the late stage of AD, and when is the optimal time for therapeutic intervention during the pathological stages of AD. A report revealed that lipopolysaccharide (LPS)-induced release of TNFα from microglia was not affected by α7 nAChR agonists, and that α7 nAChR antagonist reduced LPS-induced TNFα release [53]. Consequently, further investigations are needed to examine the effects of adding α7 nAChR agonists to AD cell lines under various conditions, or administering to animal models of AD manifesting various stages of progression and evaluating spatial learning and memory, immunohistochemistry and biochemical analysis.

ACKNOWLEDGMENTS

We are especially grateful to Dr. Masanori Sasaki, Dr. Osamu Honmou, and Dr. Nobuhiro Mikuni for enormous help throughout this study.

This study was supported in part by the Grant-in-Aid for Challenging Exploratory Research No. 23659460 (S.S.) and 24659352 (A.M.) by Japan Society for the Promotion of Science (JSPS), Grant-in-Aid for Scientific Research (B) No. 22390180 (S.S.) by JSPS, Grant-in-Aid for Scientific Research (C) No. 24590222 (K.T.) and 25460109 (Y.K.) by JSPS, and the grants by the Smoking Research Foundation (S.S. and Y.K.).

Authors' disclosures available online (http://www.j-alz.com/disclosures/view.php?id=2530).

SUPPLEMENTARY MATERIAL

The supplementary material is available in the electronic version of this article: http://dx.doi.org/10.3233/JAD-141572.

REFERENCES

[1] Hardy J, Selkoe DJ (2002) The amyloid hypothesis of Alzheimer's disease: Progress and problems on the road to therapeutics. *Science* **297**, 353-356.

[2] Akiyama H, Barger S, Barnum S, Bradt B, Bauer J, Cole GM, Cooper NR, Eikelenboom P, Emmerling M, Fiebich BL, Finch CE, Frautschy S, Griffin WS, Hampel H, Hull M, Landreth G, Lue L, Mrak R, Mackenzie IR, McGeer PL, O'Banion MK, Pachter J, Pasinetti G, Plata-Salaman C, Rogers J, Rydel R, Shen Y, Streit W, Strohmeyer R, Tooyoma I, Van Muiswinkel FL, Veerhuis R, Walker D, Webster S, Wegrzyniak B, Wenk G, Wyss-Coray T (2000) Inflammation and Alzheimer's disease. *Neurobiol Aging* **21**, 383-421.

[3] Dickson DW, Lee SC, Mattiace LA, Yen SH, Brosnan C (1993) Microglia and cytokines in neurological disease, with special reference to AIDS and Alzheimer's disease. *Glia* **7**, 75-83.

[4] McGeer PL, McGeer EG (1995) The inflammatory response system of brain: Implications for therapy of Alzheimer and other neurodegenerative diseases. *Brain Res Brain Res Rev* **21**, 195-218.

[5] Paresce DM, Ghosh RN, Maxfield FR (1996) Microglial cells internalize aggregates of the Alzheimer's disease amyloid beta-protein via a scavenger receptor. *Neuron* **17**, 553-565.

[6] Paresce DM, Chung H, Maxfield FR (1997) Slow degradation of aggregates of the Alzheimer's disease amyloid beta-protein by microglial cells. *J Biol Chem* **272**, 29390-29397.

[7] Akiyama H, Mori H, Saido T, Kondo H, Ikeda K, McGeer PL (1999) Occurrence of the diffuse amyloid beta-protein (Abeta) deposits with numerous Abeta-containing glial cells in the cerebral cortex of patients with Alzheimer's disease. *Glia* **25**, 324-331.

[8] Kakimura J, Kitamura Y, Takata K, Umeki M, Suzuki S, Shibagaki K, Taniguchi T, Nomura Y, Gebicke-Haerter PJ, Smith MA, Perry G, Shimohama S (2002) Microglial activation and amyloid-beta clearance induced by exogenous heat-shock proteins. *FASEB J* **16**, 601-603.

[9] Kitamura Y, Shibagaki K, Takata K, Tsuchiya D, Taniguchi T, Gebicke-Haerter PJ, Miki H, Takenawa T, Shimohama S (2003) Involvement of Wiskott-Aldrich syndrome protein family verprolin-homologous protein (WAVE) and Rac1 in the phagocytosis of amyloid-beta(1-42) in rat microglia. *J Pharmacol Sci* **92**, 115-123.

[10] Takata K, Kitamura Y, Yanagisawa D, Morikawa S, Morita M, Inubushi T, Tsuchiya D, Chishiro S, Saeki M, Taniguchi T, Shimohama S, Tooyama I (2007) Microglial transplantation increases amyloid-beta clearance in Alzheimer model rats. *FEBS Lett* **581**, 475-478.

[11] Schenk D, Barbour R, Dunn W, Gordon G, Grajeda H, Guido T, Hu K, Huang J, Johnson-Wood K, Khan K, Kholodenko D, Lee M, Liao Z, Lieberburg I, Motter R, Mutter L, Soriano F, Shopp G, Vasquez N, Vandevert C, Walker S, Wogulis M, Yednock T, Games D, Seubert P (1999) Immunization with amyloid-beta attenuates Alzheimer-disease-like pathology in the PDAPP mouse. *Nature* **400**, 173-177.

[12] Bard F, Cannon C, Barbour R, Burke RL, Games D, Grajeda H, Guido T, Hu K, Huang J, Johnson-Wood K, Khan K, Kholodenko D, Lee M, Lieberburg I, Motter R, Nguyen M, Soriano F, Vasquez N, Weiss K, Welch B, Seubert P, Schenk D, Yednock T (2000) Peripherally administered antibodies against amyloid beta-peptide enter the central nervous system and reduce pathology in a mouse model of Alzheimer disease. *Nat Med* **6**, 916-919.

[13] Janus C, Pearson J, McLaurin J, Mathews PM, Jiang Y, Schmidt SD, Chishti MA, Horne P, Heslin D, French J, Mount HT, Nixon RA, Mercken M, Bergeron C, Fraser PE, St George-Hyslop P, Westaway D (2000) A beta peptide immunization reduces behavioural impairment and plaques in a model of Alzheimer's disease. *Nature* **408**, 979-982.

[14] Morgan D, Diamond DM, Gottschall PE, Ugen KE, Dickey C, Hardy J, Duff K, Jantzen P, DiCarlo G, Wilcock D, Connor K, Hatcher J, Hope C, Gordon M, Arendash GW (2000) A beta peptide vaccination prevents memory loss in an animal model of Alzheimer's disease. *Nature* **408**, 982-985.

[15] Nordberg A, Hellstrom-Lindahl E, Lee M, Johnson M, Mousavi M, Hall R, Perry E, Bednar I, Court J (2002) Chronic nicotine treatment reduces beta-amyloidosis in the brain of a mouse model of Alzheimer's disease (APPsw). *J Neurochem* **81**, 655-658.

[16] Hellstrom-Lindahl E, Court J, Keverne J, Svedberg M, Lee M, Marutle A, Thomas A, Perry E, Bednar I, Nordberg A (2004) Nicotine reduces A beta in the brain and cerebral vessels of APPsw mice. *Eur J Neurosci* **19**, 2703-2710.

[17] Court JA, Johnson M, Religa D, Keverne J, Kalaria R, Jaros E, McKeith IG, Perry R, Naslund J, Perry EK (2005) Attenuation of Abeta deposition in the entorhinal cortex of normal elderly individuals associated with tobacco smoking. *Neuropathol Appl Neurobiol* **31**, 522-535.

[18] Shytle RD, Mori T, Townsend K, Vendrame M, Sun N, Zeng J, Ehrhart J, Silver AA, Sanberg PR, Tan J (2004) Cholinergic modulation of microglial activation by alpha 7 nicotinic receptors. *J Neurochem* **89**, 337-343.

[19] Suzuki T, Hide I, Matsubara A, Hama C, Harada K, Miyano K, Andra M, Matsubayashi H, Sakai N, Kohsaka S, Inoue K, Nakata Y (2006) Microglial alpha7 nicotinic acetylcholine receptors drive a phospholipase C/IP3 pathway and modulate the cell activation toward a neuroprotective role. *J Neurosci Res* **83**, 1461-1470.

[20] Takata K, Kitamura Y, Saeki M, Terada M, Kagitani S, Kitamura R, Fujikawa Y, Maelicke A, Tomimoto H, Taniguchi T, Shimohama S (2010) Galantamine-induced amyloid-{beta} clearance mediated via stimulation of microglial nicotinic acetylcholine receptors. *J Biol Chem* **285**, 40180-40191.

[21] Suzuki S, Kawamata J, Matsushita T, Matsumura A, Hisahara S, Takata K, Kitamura Y, Kem W, Shimohama S (2013) 3-[(2,4-Dimethoxy)benzylidene]-anabaseine dihydrochloride protects against 6-hydroxydopamine-induced parkinsonian neurodegeneration through alpha7 nicotinic acetylcholine receptor stimulation in rats. *J Neurosci Res* **91**, 462-471.

[22] Kawahara K, Suenobu M, Yoshida A, Koga K, Hyodo A, Ohtsuka H, Kuniyasu A, Tamamaki N, Sugimoto Y, Nakayama H (2012) Intracerebral microinjection of interleukin-4/interleukin-13 reduces beta-amyloid accumulation in the ipsilateral side and improves cognitive deficits in young amyloid precursor protein 23 mice. *Neuroscience* **207**, 243-260.

[23] Bachstetter AD, Norris CM, Sompol P, Wilcock DM, Goulding D, Neltner JH, St Clair D, Watterson DM, Van Eldik LJ (2012) Early stage drug treatment that normalizes proinflammatory cytokine production attenuates synaptic dysfunction in a mouse model that exhibits age-dependent progression of Alzheimer's disease-related pathology. *J Neurosci* **32**, 10201-10210.

[24] Kulkarni AP, Pillay NS, Kellaway LA, Kotwal GJ (2008) Intracranial administration of vaccinia virus complement control protein in Mo/Hu APPswe PS1dE9 transgenic mice at an

early age shows enhanced performance at a later age using a cheese board maze test. *Biogerontology* **9**, 405-420.

[25] Aso E, Semakova J, Joda L, Semak V, Halbaut L, Calpena A, Escolano C, Perales JC, Ferrer I (2013) Triheptanoin supplementation to ketogenic diet curbs cognitive impairment in APP/PS1 mice used as a model of familial Alzheimer's disease. *Curr Alzheimer Res* **10**, 290-297.

[26] Sperling RA, Aisen PS, Beckett LA, Bennett DA, Craft S, Fagan AM, Iwatsubo T, Jack CR Jr, Kaye J, Montine TJ, Park DC, Reiman EM, Rowe CC, Siemers E, Stern Y, Yaffe K, Carrillo MC, Thies B, Morrison-Bogorad M, Wagster MV, Phelps CH (2011) Toward defining the preclinical stages of Alzheimer's disease: Recommendations from the National Institute on Aging-Alzheimer's Association workgroups on diagnostic guidelines for Alzheimer's disease. *Alzheimers Dement* **7**, 280-292.

[27] Graeber MB, Streit WJ, Kiefer R, Schoen SW, Kreutzberg GW (1990) New expression of myelomonocytic antigens by microglia and perivascular cells following lethal motor neuron injury. *J Neuroimmunol* **27**, 121-132.

[28] Slepko N, Levi G (1996) Progressive activation of adult microglial cells *in vitro*. *Glia* **16**, 241-246.

[29] Perego C, Fumagalli S, De Simoni MG (2011) Temporal pattern of expression and colocalization of microglia/macrophage phenotype markers following brain ischemic injury in mice. *J Neuroinflammation* **8**, 174.

[30] Park BG, Lee JS, Lee JY, Song DY, Jeong SW, Cho BP (2011) Co-localization of activating transcription factor 3 and phosphorylated c-Jun in axotomized facial motoneurons. *Anat Cell Biol* **44**, 226-237.

[31] Lee JK, Jin HK, Bae JS (2009) Bone marrow-derived mesenchymal stem cells reduce brain amyloid-beta deposition and accelerate the activation of microglia in an acutely induced Alzheimer's disease mouse model. *Neurosci Lett* **450**, 136-141.

[32] Takata K, Kitamura Y, Tsuchiya D, Kawasaki T, Taniguchi T, Shimohama S (2004) High mobility group box protein-1 inhibits microglial Abeta clearance and enhances Abeta neurotoxicity. *J Neurosci Res* **78**, 880-891.

[33] Kaneko I, Tutumi S (1997) Conformations of β-amyloid in solution. *J Neurochem* **68**, 437-439.

[34] Kawarabayashi T, Younkin LH, Saido TC, Shoji M, Ashe KH, Younkin SG (2001) Age-dependent changes in brain, CSF, and plasma amyloid (beta) protein in the Tg2576 transgenic mouse model of Alzheimer's disease. *J Neurosci* **21**, 372-381.

[35] Bishop GM, Robinson SR (2003) Deposits of fibrillar A beta do not cause neuronal loss or ferritin expression in adult rat brain. *J Neural Transm* **110**, 381-400.

[36] Garcia-Alloza M, Robbins EM, Zhang-Nunes SX, Purcell SM, Betensky RA, Raju S, Prada C, Greenberg SM, Bacskai BJ, Frosch MP (2006) Characterization of amyloid deposition in the APPswe/PS1dE9 mouse model of Alzheimer disease. *Neurobiol Dis* **24**, 516-524.

[37] Ruan L, Kang Z, Pei G, Le Y (2009) Amyloid deposition and inflammation in APPswe/PS1dE9 mouse model of Alzheimer's disease. *Curr Alzheimer Res* **6**, 531-540.

[38] Streit WJ, Xue QS (2009) Life and death of microglia. *J Neuroimmune Pharmacol* **4**, 371-379.

[39] Milligan CE, Cunningham TJ, Levitt P (1991) Differential immunochemical markers reveal the normal distribution of brain macrophages and microglia in the developing rat brain. *J Comp Neurol* **314**, 125-135.

[40] Milligan CE, Levitt P, Cunningham TJ (1991) Brain macrophages and microglia respond differently to lesions of the developing and adult visual system. *J Comp Neurol* **314**, 136-146.

[41] Graeber MB, Lopez-Redondo F, Ikoma E, Ishikawa M, Imai Y, Nakajima K, Kreutzberg GW, Kohsaka S (1998) The microglia/macrophage response in the neonatal rat facial nucleus following axotomy. *Brain Res* **813**, 241-253.

[42] Maezawa I, Hong HS, Liu R, Wu CY, Cheng RH, Kung MP, Kung HF, Lam KS, Oddo S, Laferla FM, Jin LW (2008) Congo red and thioflavin-T analogs detect Abeta oligomers. *J Neurochem* **104**, 457-468.

[43] Hickman SE, Allison EK, El Khoury J (2008) Microglial dysfunction and defective beta-amyloid clearance pathways in aging Alzheimer's disease mice. *J Neurosci* **28**, 8354-8360.

[44] Krabbe G, Halle A, Matyash V, Rinnenthal JL, Eom GD, Bernhardt U, Miller KR, Prokop S, Kettenmann H, Heppner FL (2013) Functional impairment of microglia coincides with Beta-amyloid deposition in mice with Alzheimer-like pathology. *PLoS One* **8**, e60921.

[45] Moreno H, Yu E, Pigino G, Hernandez AI, Kim N, Moreira JE, Sugimori M, Llinas RR (2009) Synaptic transmission block by presynaptic injection of oligomeric amyloid beta. *Proc Natl Acad Sci U S A* **106**, 5901-5906.

[46] Pigino G, Morfini G, Atagi Y, Deshpande A, Yu C, Jungbauer L, LaDu M, Busciglio J, Brady S (2009) Disruption of fast axonal transport is a pathogenic mechanism for intraneuronal amyloid beta. *Proc Natl Acad Sci U S A* **106**, 5907-5912.

[47] Umeda T, Tomiyama T, Sakama N, Tanaka S, Lambert MP, Klein WL, Mori H (2011) Intraneuronal amyloid beta oligomers cause cell death via endoplasmic reticulum stress, endosomal/lysosomal leakage, and mitochondrial dysfunction *in vivo*. *J Neurosci Res* **89**, 1031-1042.

[48] Frenkel D, Wilkinson K, Zhao L, Hickman SE, Means TK, Puckett L, Farfara D, Kingery ND, Weiner HL, El Khoury J (2013) Scara1 deficiency impairs clearance of soluble amyloid-beta by mononuclear phagocytes and accelerates Alzheimer's-like disease progression. *Nat Commun* **4**, 2030.

[49] Mandrekar S, Jiang Q, Lee CY, Koenigsknecht-Talboo J, Holtzman DM, Landreth GE (2009) Microglia mediate the clearance of soluble Abeta through fluid phase macropinocytosis. *J Neurosci* **29**, 4252-4262.

[50] De Simone R, Ajmone-Cat MA, Carnevale D, Minghetti L (2005) Activation of alpha7 nicotinic acetylcholine receptor by nicotine selectively up-regulates cyclooxygenase-2 and prostaglandin E2 in rat microglial cultures. *J Neuroinflammation* **2**, 4.

[51] Parada E, Egea J, Buendia I, Negredo P, Cunha AC, Cardoso S, Soares MP, Lopez MG (2013) The microglial alpha7-acetylcholine nicotinic receptor is a key element in promoting neuroprotection by inducing heme oxygenase-1 via nuclear factor erythroid-2-related factor 2. *Antioxid Redox Signal* **19**, 1135-1148.

[52] Mencel M, Nash M, Jacobson C (2013) Neuregulin upregulates microglial alpha7 nicotinic acetylcholine receptor expression in immortalized cell lines: Implications for regulating neuroinflammation. *PLoS One* **8**, e70338.

[53] Thomsen MS, Mikkelsen JD (2012) The alpha7 nicotinic acetylcholine receptor ligands methyllycaconitine, NS6740 and GTS-21 reduce lipopolysaccharide-induced TNF-alpha release from microglia. *J Neuroimmunol* **251**, 65-72.

Neuroscience Letters 584 (2015) 276–281

Contents lists available at ScienceDirect

Neuroscience Letters

journal homepage: www.elsevier.com/locate/neulet

Intravenous mesenchymal stem cell administration exhibits therapeutic effects against 6-hydroxydopamine-induced dopaminergic neurodegeneration and glial activation in rats

Syuuichirou Suzuki[a], Jun Kawamata[a], Naoyuki Iwahara[a], Akihiro Matsumura[a], Shin Hisahara[a], Takashi Matsushita[b], Masanori Sasaki[c], Osamu Honmou[c], Shun Shimohama[a,*]

[a] Department of Neurology, School of Medicine, Sapporo Medical University, Sapporo, Japan
[b] Department of Neurology, Yale University School of Medicine, New Haven, USA
[c] Department of Neural Regenerative Medicine, Research Institute for Frontier Medicine, Sapporo Medical University, Sapporo, Japan

HIGHLIGHTS

- Intravenous administration of hBM-MSCs prevented 6-OHDA-induced rotation behavior.
- Protection from DA degeneration was accompanied by inhibition of glial activation.
- This is the first report showing hBM-MSCs improved explicit PD symptom with 6-OHDA.

ARTICLE INFO

Article history:
Received 3 October 2014
Received in revised form 22 October 2014
Accepted 22 October 2014
Available online 1 November 2014

Keywords:
Mesenchymal stem cell
Neuroprotection
Anti-inflammatory
6-Hydroxydopamine
Parkinson's disease

ABSTRACT

To explore a novel therapy against Parkinson's disease (PD), we evaluated the therapeutic effects of human bone marrow-derived mesenchymal stem cells (hBM-MSCs), pluripotent stromal cells with secretory potential of various neurotrophic and anti-inflammatory factors, in a hemi-parkinsonian rat model. The unilateral intrastriatal 6-hydroxydopamine (6-OHDA)-lesioned rats were injected hBM-MSCs (1.0×10^7 cells) or PBS intravenously 16 days after lesioning. Administration of hBM-MSCs inhibited methamphetamine-stimulated rotational behavior at 7, 14, 21 and 28 days after transplantation. Immunohistochemical analysis also showed that number of TH-positive neurons in the substantia nigra pars compacta was significantly preserved in hBM-MSCs-transplanted rats compared to sham-operated rats, whereas the immunoreactivity of ionized calcium binding adaptor molecule 1 was markedly inhibited. In this study, we demonstrated the therapeutic effects of intravenous hBM-MSCs administration in parkinsonian model rats presenting distinct parkinsonian phenotype at 16 days after 6-OHDA lesioning. The favorable findings raise the possibility that hBM-MSCs could be a novel therapeutic option to promote survival of dopaminergic neurons in PD.

1. Introduction

Parkinson's disease (PD) is one of the major progressive neurodegenerative diseases and the pathologic feature is a selective loss of nigral dopaminergic neurons causing characteristic movement disturbances such as muscle rigidity, resting tremor, bradykinesia and postural instability [20]. Remediation of PD by dopamine replacement therapy, which has been used mainly for ameliorating movement disturbances in PD, does not prevent progression. Many neuroprotective compounds have been tested in PD models, but most were administered before or at the same time as lesioning [17,21].

Cell therapy was developed as an alternative tool for the treatment of PD. Neural stem cells [11], fetal mesencephalic neurons [7] and embryonic stem cells [18] have been reported as candidates for cell therapy against PD. However, there are ethical problems about the use of embryonic and fetal tissues. These cells also are exhaustible and relatively difficult to prepare. Our group

* Corresponding author at: Department of Neurology, School of Medicine, Sapporo Medical University, South 1, West 16, Chuo-ku, Sapporo 060-8543, Japan. Tel.: +81 11 611 2111; fax: +81 11 622 7668.
E-mail address: shimoha@sapmed.ac.jp (S. Shimohama).

http://dx.doi.org/10.1016/j.neulet.2014.10.039
0304-3940/

previously reported the beneficial effects of intravenous delivery of human bone marrow-derived mesenchymal stem cells (hBM-MSCs) into rotenone-treated mice [10]. In that study, we confirmed that hBM-MSC expressed several neurotrophic factors and elicited endogenous brain repair mechanisms. We hypothesized that the therapeutic properties of hBM-MSCs may also be derived from suppressing neuroinflammation in addition to the reported functional characteristics of hBM-MSCs.

To evaluate the hypothesis, we investigated the therapeutic effects of intravenous injection of hBM-MSCs in a 6-hydroxydopamine (6-OHDA)-induced hemi-parkinsonian rat model. Using symptomatic parkinsonian model rats at 16 days after lesion induction, we confirmed that MSCs-induced neuroprotection was accompanied by inhibition of 6-OHDA-evoked glial activation.

2. Materials and methods

2.1. Expansion of hBM-MSCs

Human BM-MSCs (Takara Bio, Otsu, Japan) were expanded according to supplier's instructions. Dulbecco's modified Eagle's medium (DMEM) (Sigma, St. Louis, MO) supplemented with 10% heat-inactivated fetal bovine serum (FBS) (Gibco BRL, Grand Island, NY), 2 mM L-glutamine (Sigma), 100 U/ml penicillin and 0.1 mg/ml streptomycin (Gibco BRL) was used as the culture medium. The seeding density was approximately 4000 cells/cm^2. The cells were plated on 55 or 150 cm^2 tissue culture dish (Iwaki, Tokyo, Japan), and incubated in a humidified atmosphere of 5% CO_2 at 37 °C. When cultures reached sub-confluence (80–90% confluence), the adherent cells were detached with trypsin–EDTA solution (Sigma) and subcultured at 4000–5000 cells/cm^2. In this study, we used hBM-MSCs up to six passages.

2.2. Hemi-parkinsonian rat model and transplantation

The animal studies were approved by the Animal Care and Use Committee of Sapporo Medical University. All procedures were carried out in accordance with the institutional guidelines.

Nine-week-old female Sprague–Dawley rats, ranging in weight from 200 to 240 g, were purchased from Sankyo Labo Service Corporation Inc. (Tokyo, Japan). Rats were housed in a temperature-controlled environment at 25°C under a 12 h light/dark cycle and given *ad libitum* access to food and water.

For stereotaxic microinjection, a rat was anesthetized with ketamine (30 mg/kg) and xylazine (7.5 mg/kg) *i.p.* and immobilized in a stereotaxic frame. Subsequently, 6-OHDA hydrobromide (Sigma, St. Louis, MO, 40 nmol) in a final volume of 5 μL of sterilized physiological saline containing 0.02% ascorbic acid (4.4 nmol, as a 6-OHDA stabilizer) was injected into the left striatum. According to the rat brain atlas [16], the injection coordinates were: (1) 0.5 mm anterior–posterior, 2.5 mm left lateral, and 5 mm ventral; and (2) −0.5 mm anterior–posterior, 4.2 mm left lateral, and 5 mm ventral from the bregma with the incisor bar set at −3 mm, corresponding to dorsomedial and ventrolateral striatum, respectively. Injection was delivered using a motor-driven 1 μL Hamilton syringe with a 26-gauge needle. The infusion rate was 1 μL/min, and the needle was retained for a further 5 min after injection. Behavioral analyses were performed 14 days after 6-OHDA injection (day −2). Rats with a rotation rate ranging from 6 to 20 turns/min were considered to be an established PD model and were used in this study.

For transplantation, hBM-MSCs (1.0×10^7 cells/animal) were injected into the femoral vein of a 6-OHDA-lesioned rat on day 0 (Fig. 1). The number of transplanted hBM-MSCs was decided according to the previous report [22]. Sham-operated rats received

A Model production and transplantation

Group	6-OHDA	PBS or Approx.number of grafted cells	n
PBS	+	0.5 ml PBS	19
MSCs	+	1.0×10^7 cells in 0.5 ml PBS	13

B Schematic diagram of the protocol

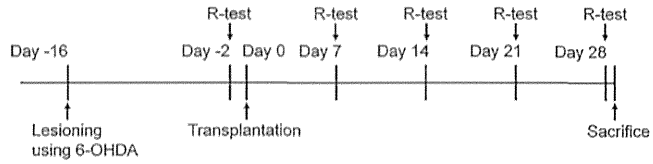

Fig. 1. Experimental design. (A) Model production and transplantation. 6-OHDA was micro-injected into the left striatum of SD rats to produce hemi-parkinsonian models. The rats were divided into two groups (MSCs group, $n = 19$; PBS group, $n = 13$). For transplantation, MSCs (1.0×10^7 cells/animal) were administered to 6-OHDA-lesioned rat by injection into the femoral vein. (B) Schematic diagram of the protocol. Rotational behavior was assessed at day 14 after 6-OHDA injection. Methamphetamine (3.0 mg/kg) was injected *i.p.* and the number of full 360° rotations in ipsilateral direction was counted for 120 min. Rats with a rotation frequency ranging from 6 to 20 turns/min were defined as PD model rats. Thereafter, behavioral analyses were performed on days 7, 14, 21 and 28. On day 29, the rats were sacrificed and brains were quickly removed for immunohistochemical analyses. 6-OHDA, 6-hydroxydopamine; MSCs, human bone marrow-derived mesenchymal stem cells; R-test, rotational behavior test.

PBS injection. All rats including sham-operated rats were injected daily with cyclosporine (10 mg/kg, *i.p.*) beginning 7 days after lesion induction. One day after the last behavioral analysis (day 29), all rats were sacrificed for immunohistochemical assessments.

2.3. Behavioral analysis

Rats in the hBM-MSCs and PBS groups were administered methamphetamine (Dainippon Sumitomo Pharma, Osaka, Japan, 3.0 mg/kg, *i.p.*) to provoke dopamine release from the dopaminergic nerve terminals. Drug-induced rotational asymmetry was assessed in rotometer bowls, as described previously [20,24]. The number of full body turn rotations in ipsilateral direction was counted for 120 min after methamphetamine administration. Behavioral analyses were performed on day −2 and days 7, 14, 21 and 28.

2.4. Immunohistochemistry

One day after the final test for methamphetamine-induced rotational behavior (day 29), the rats were deeply anesthetized with ketamine (40 mg/kg) and xylazine (10 mg/kg) *i.p.* and perfused through the aorta with 200 ml of 10 mM phosphate-buffered saline (PBS), followed by 200 ml of a cold fixative containing 4% paraformaldehyde in 100 mM phosphate buffer (PB). After perfusion, the brain was quickly removed and postfixed for 2 days with 4% paraformaldehyde in 10 mM PB, and then transferred to 10% sucrose followed by 20% sucrose in 10 mM PBS at 4 °C. The brain was cut into 60-μm-thick slices using a cryostat and collected in 10 mM PBS containing 0.3% Triton X-100 (PBS-T). Brain slices were incubated with primary antibodies; rabbit polyclonal antibodies against tyrosine hydroxylase (TH, Millipore, Bedford, MA 1:10,000) and against ionized calcium binding adaptor molecule 1 (Iba1, Wako Chemical, Osaka, Japan, 1:5000), for 3 days at 4 °C. After several washes, sections were incubated with biotinylated anti-rabbit IgG for 2 h at room temperature. The sections were then incubated with 1:4000 avidin peroxidase (ABC Elite Kit; Vector Laboratories, Burlingame, CA) for 1 h at room temperature. All the sections were washed several times with PBS-T after each incubation. Labeling

was visualized by incubating with 3,3′-diaminobenzidine (DAB) and nickel ammonium, yielding a dark blue color [24].

2.5. Stereological analysis

The numbers of TH-immunoreactive (TH^+) neurons in the substantia nigra pars compacta (SNpc) were estimated using Stereo Investigator software (MBF Bioscience, Williston, VT) and stereologic principles. Six sections (60-μm-thick), each separated by 240 μm from the anterior to the posterior midbrain, were used for counting in each rat. A Zeiss AxioPhot 2 (Carl Zeiss) was coupled to an Optronics MicroFire digital camera CX9000 (MBF Bioscience) for visualization of tissue sections. The total number of TH^+ neurons was estimated from coded slides using the optical fractionator method. For each tissue section analyzed, the section thickness was assessed empirically and 5-μm-thick guard zones were used at the top and bottom of each section. The SNpc was outlined under low magnification (4×) and 10 sites in the outlined region were analyzed using a systematic random sampling design with a grid size of 180 μm × 180 μm (including the frame size) and a dissector height of 20 μm. Neurons were counted under 40× magnification.

2.6. Densitometric analysis

To evaluate the Iba1-immunolabeled microglial reactivity, the dorsomedial striatum sections at the site of 6-OHDA injection were digitized using a Nikon AZ100 microscope and a Q Imaging camera. The Images were converted to black and white by Adobe Photoshop CS5.1 (Adobe Systems Inc.) and opened in ImageJ (NIH) for analysis. The area of microglial immunostaining was determined by ImageJ, which provided the absolute area of microglial immunolabeling within each image [23].

2.7. Statistical evaluation

Drug-induced rotational asymmetry, the number of TH^+ neurons, the OD of the striatum and Iba1 immunostaining area are presented as mean ± standard error of the mean (SEM). The differences between groups were analyzed by Student's *t*-test. The JMP statistical program (SAS Institute Inc., Cary, NC) was used for data analysis.

3. Results

3.1. Human BM-MSC transplantation reduced methamphetamine-induced rotation behavior

In methamphetamine-induced rotation test (Fig. 2), hBM-MSCs transplantation significantly reduced the number of rotations per minute over time, compared to PBS treatment (MSC group: 11.2 ± 0.8, 8.6 ± 1.0, 9.4 ± 1.4 and 9.0 ± 1.3 turns/min; PBS group: 14.7 ± 1.0, 16.0 ± 1.4, 16.6 ± 1.3 and 15.7 ± 1.6 turns/min on days 7, 14, 21 and 28, respectively. Student's *t*-test for MSCs group *vs.* PBS group: $P < 0.05$ on days 7 and 28; $P < 0.01$ on days 14 and 21). Thus, drug-induced rotation behavior was ameliorated in MSCs group compared to PBS group, with significant differences.

3.2. Human BM-MSCs transplantation increased TH immunohistochemical staining in the substantia nigra

Tyrosine hydroxylase, a rate-limiting enzyme in catecholamine synthesis, is a marker of dopaminergic neurons in the central nervous system (CNS) [6]. Stereotaxic microinjection of 6-OHDA into the striatum induced massive losses of TH^+ neurons in the ipsilateral SNpc. Human BM-MSCs transplantation markedly preserved TH^+ neurons in the SNpc (Fig. 3C and D). Semiquantitative analysis of nigral TH^+ neurons showed that hBM-MSCs significantly protected TH^+ neurons compared to PBS (Fig. 3E). These results indicate that hBM-MSCs transplantation protected against 6-OHDA-induced loss of dopaminergic neurons in the SNpc.

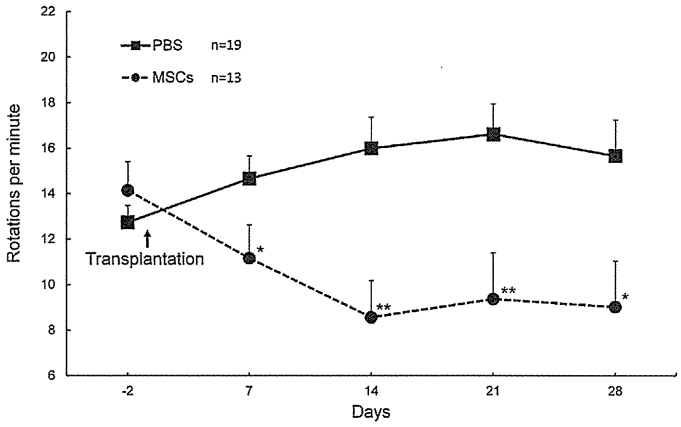

Fig. 2. Methamphetamine-induced rotational behavior in 6-OHDA-treated rats with or without MSC transplantation. MSCs were administered to 6-OHDA-lesioned rat. Rotational behavior was assessed on day 2 before and days 7, 14, 21 and 28 after transplantation ($n = 13$, solid circles). PBS was given to sham-operated rats ($n = 19$, solid squares). Data are expressed as mean ± SEM. $^*P < 0.05$, $^{**}P < 0.01$, MSCs group *vs.* PBS group by Student's *t*-test.

3.3. Human BM-MSCs suppressed glial activation in 6-OHDA-lesioned rats

To investigate other effects of hBM-MSC in 6-OHDA-lesioned rats, we examined Iba1 immunoreactivity in the dorsomedial striatum of rats injected with 6-OHDA (Fig. 4A and B). Iba1 is a general marker for microglia in both resting and activated states. In the dorsomedial striatum of the MSCs group, immunoreactivity to Iba1 was detected in resting microglia with small cell bodies and highly branched and thinner processes. On the contrary, microglia changed into an activated state with thickened and retracted processes in the PBS group. The degree of microglial reactivity was quantified by measuring the area occupied by microglia showing Iba1 immunoreactivity within a selected area (4 mm × 1.5 mm). The average immunolabeled area in the hBM-MSCs group (1.85 ± 0.24 mm^2) was significantly smaller compared to that of the PBS group (2.37 ± 0.09 mm^2) (Fig. 4C).

4. Discussion

In this study, we used intrastriatal 6-OHDA-lesioned rat as an animal model of PD. Microinjection of 6-OHDA directly into the substantia nigra, medial forebrain bundle or striatum causes selective destruction of nigrostriatal dopaminergic neurons *via* the dopaminergic transporter. Although the primary damage created by striatal infusion of 6-OHDA was confined to the nigrostriatal dopaminergic neurons, the loss of nigrostriatal dopaminergic neurons is more progressively accompanied by microglial activation compared to injection into substantia nigra or medial forebrain bundle [8]. Sauer and Oertel [19] showed that injection of 6-OHDA into the striatum causes a progressive degeneration of dopaminergic neurons in the substantia nigra, starting between 1 and 2 weeks after lesion induction and continuing over 8–16 weeks. As a preliminary test of this model, we confirmed that methamphetamine-induced rotation frequency remained elevated (9.7 ± 2.1 turns/min) in the model rats up to 14 weeks, and that dopaminergic neurons in the substantia nigra decreased to 19.4 ± 0.50% compared to the contralateral side at the end of the observation period (data not shown). However, the

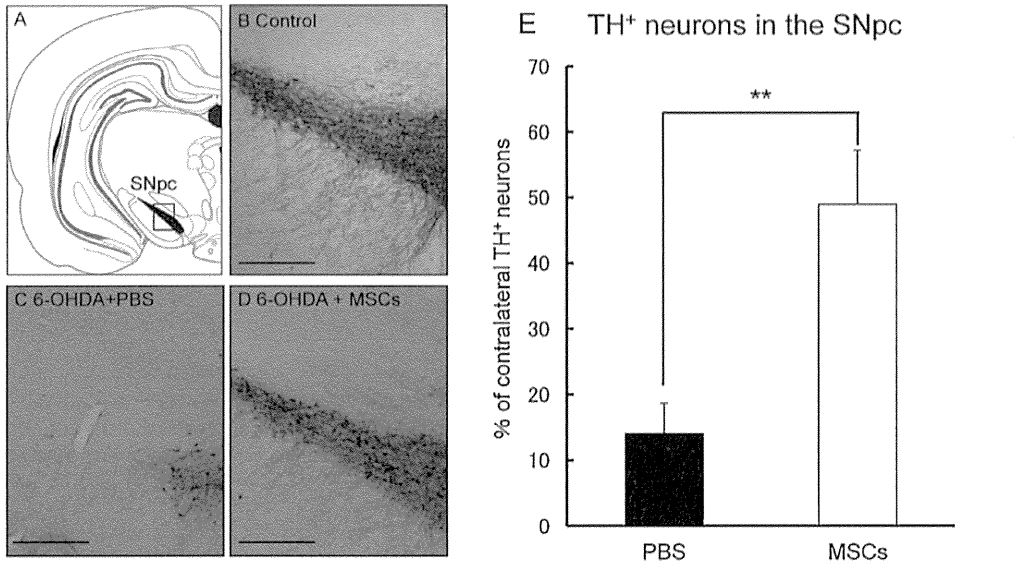

Fig. 3. (A) Schematic representation of the substantia nigra pars compacta (SNpc: black area). (B–D) Representative photomicrographs of TH^+ neurons in SNpc. Scale bar: 200 μm. (B) Control rat (that with neither previous 6-OHDA injection nor treatment). (E) Stereological analysis of TH^+ neurons in SNpc. Data are expressed as mean ± SEM of percent number of TH^+ neurons relative to contralateral side in ipsilateral nigral sections. $^{**}P < 0.01$, Student's *t*-test.

methamphetamine-induced rotational frequency peaked at 5–6 weeks after 6-OHDA injection, then declining gradually over the following weeks. We therefore planned a total observation period of 44 days after 6-OHDA injection for this study.

The present study demonstrated that hBM-MSCs treatment significantly inhibited both methamphetamine-stimulated rotation and dopaminergic neuronal loss. Several studies using *in vitro* or *in vivo* PD models have shown that MSCs prevent degeneration of nigrostriatal dopaminergic neurons. Study has demonstrated that MSCs have the capability to differentiate into dopaminergic neurons and show therapeutic ability for PD [4]. In addition, studies using animal PD models with rotenone or MG-132, a proteasome inhibitor, have shown that intravenously injected MSCs migrated into lesions in the brain and exhibited TH immunoreactivity [10,15]. Another study injected hBM-MSCs intravenously into 6-OHDA-induced parkinsonian model rats, and detected some of the injected hBM-MSCs in rat brain at 2 days after transplantation, fewer at 1 week, and none at 4 weeks [22]. However, in the present study, survival of the transplanted hBM-MSCs was not detected using anti-human nuclei staining. In addition, using hBM-MSCs pre-labeled with fluorescent dye (CellView), we were not able to detect the transplanted hBM-MSCs at the

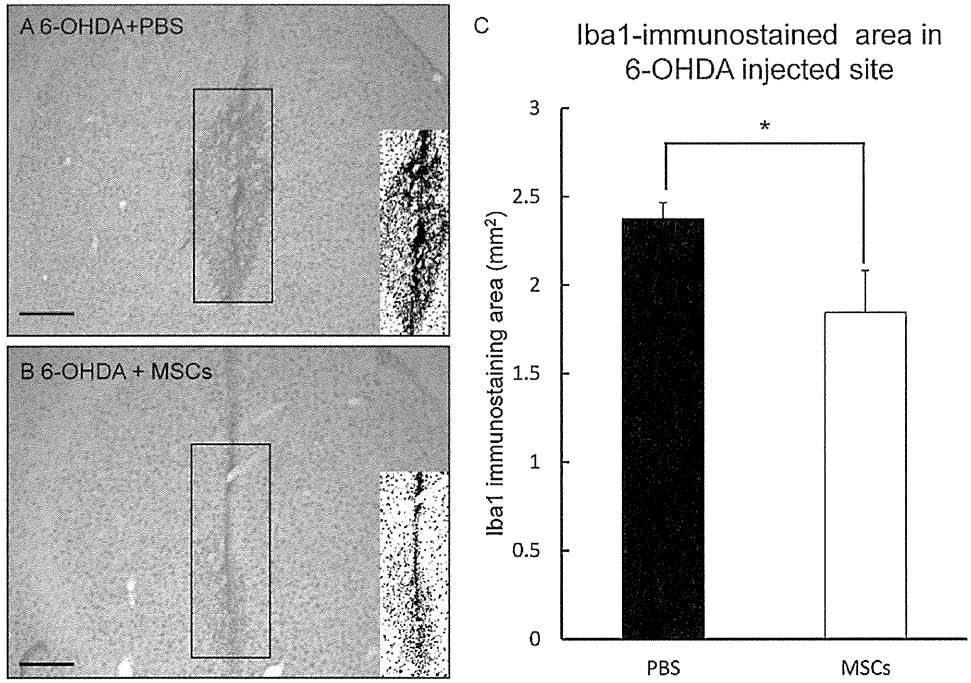

Fig. 4. (A and B) Representative photomicrographs of Iba1 immunoreactivity in the striatum. Scale bar 1 mm. (C) Degree of microglial reactivity assessed by area of Iba1 immunostaining. Data are expressed as mean ± SEM of Iba1-immunostained area in sections. $^{*}P < 0.05$, Student's *t*-test.

nigrostriatal sections of 6-OHDA-lesioned rat at 7 days after hBM-MSC transplantation (data not shown).

There is adequate evidence that MSCs express a variety of neurotrophic factors inducing increased neuronal survival, intrinsic cell proliferation and nerve fiber regeneration. We have already shown that hBM-MSCs express nerve growth factor, glial cell line-derived neurotrophic factor, brain-derived neurotrophic factor (BDNF), insulin-like growth factor-1 and basic fibroblast growth factor at mRNA and protein levels [10,25]. Another notable neurotrophic factor, vasoactive intestinal peptide (VIP), which is also expressed in MSCs [2], significantly reduced 1-methyl-4-phenyl-1,2,3,6-tetrahydropyridine-induced microglial activation, expression of the neurotoxic factors tumor necrosis factor (TNF)-α and interleukin-1β, and enzymatic activity of iNOS and NADPH-oxidase in a PD mouse model [3]. BDNF and VIP have been reported to cross the blood-brain barrier (from blood to brain) *via* a high-capacity, saturable transport system and transmembrane diffusion, respectively [5,14].

In pathological studies of the substantia nigra from PD patients, abundant activated glial cells were observed indicating a robust inflammatory state [1], and a significant increase in density of glial cells expressing pro-inflammatory cytokines such as TNF-α, interleukin-1β and interferon-γ has been demonstrated in the basal ganglia [9]. Because microglia play a major role in brain inflammation and often contribute to neurodegeneration in PD patients, the inhibition of glial activation could be neuroprotective. In this study, a complex set of trophic factors and cytokines secreted by hBM-MSCs might have exerted neuroprotective effect on dopaminergic neurons through anti-inflammatory actions [12] that reduce oxidative stress and decrease apoptosis [13].

As mentioned above, the injected hBM-MSCs were not detected in the nigrostriatal pathway at 7 days after hBM-MSCs injection, but neuroprotective effects continued for at least 12 weeks (Supplementary Fig. S1). Even though intravenously injected hBM-MSCs do not survive or engraft for a long-term, the fact means our experimental model ensures hBM-MSCs injection is the safely therapeutic alternative avoiding malignant transformation. As repeated administrations of hBM-MSCs would be required in order to achieve a significant clinical effect in progressive PD patients, avoiding malignant transformation is crucial. Use of autologous cells is expected to avoid rejection and guarantee high level of safety without using immunosuppressant in the clinical setting.

Supplementary Fig. S1 related to this article can be found, in the online version, at http://dx.doi.org/10.1016/j.neulet.2014.10.039.

The present study confirms the therapeutic effects of intravenous hBM-MSCs administration in symptomatic parkinsonian model rats after being lesioned. Further studies are warranted to explore the clinical application of hBM-MSCs to PD patients after onset of clinical symptoms.

In conclusion, we demonstrated that hBM-MSCs have neuroprotective effects on dopaminergic neurons *via* an anti-inflammatory mechanism mediated by modulation of microglial activation. Along with various trophic effects, these anti-inflammatory properties of hBM-MSCs may have major therapeutic implications in the treatment of PD.

Acknowledgements

The authors thank Ms. Hiromi Suzuki and Ms. Ayano Yamauchi for technical assistance throughout this study. This study was supported in part by the Grant-in-Aid for Challenging Exploratory Research Nos. 23659384, 23659460 and 24659352 by Japan Society for the Promotion of Science (JSPS), Grant-in-Aid for Scientific Research (B) No. 22390180 by JSPS and the grant by the Smoking Research Foundation.

References

[1] R.B. Banati, S.E. Daniel, S.B. Blunt, Glial pathology but absence of apoptotic nigral neurons in long-standing Parkinson's disease, Mov. Disord. 13 (1998) 221–227.
[2] M. Cobo, P. Anderson, K. Benabdellah, M.G. Toscano, P. Munoz, A. Garcia-Perez, I. Gutierrez, M. Delgado, F. Martin, Mesenchymal stem cells expressing vasoactive intestinal peptide ameliorate symptoms in a model of chronic multiple sclerosis, Cell Transplant. 22 (2013) 839–854.
[3] M. Delgado, D. Ganea, Neuroprotective effect of vasoactive intestinal peptide (VIP) in a mouse model of Parkinson's disease by blocking microglial activation, FASEB J. 17 (2003) 944–946.
[4] M. Dezawa, H. Kanno, M. Hoshino, H. Cho, N. Matsumoto, Y. Itokazu, N. Tajima, H. Yamada, H. Sawada, H. Ishikawa, T. Mimura, M. Kitada, Y. Suzuki, C. Ide, Specific induction of neuronal cells from bone marrow stromal cells and application for autologous transplantation, J. Clin. Investig. 113 (2004) 1701–1710.
[5] D. Dogrukol-Ak, W.A. Banks, N. Tuncel, M. Tuncel, Passage of vasoactive intestinal peptide across the blood-brain barrier, Peptides 24 (2003) 437–444.
[6] P.R. Dunkley, L. Bobrovskaya, M.E. Graham, E.I. von Nagy-Felsobuki, P.W. Dickson, Tyrosine hydroxylase phosphorylation: regulation and consequences, J. Neurochem. 91 (2004) 1025–1043.
[7] A.O. Hebb, K. Hebb, A.C. Ramachandran, I. Mendez, Glial cell line-derived neurotrophic factor-supplemented hibernation of fetal ventral mesencephalic neurons for transplantation in Parkinson disease: long-term storage, J. Neurosurg. 98 (2003) 1078–1083.
[8] S. Hisahara, S. Shimohama, Toxin-induced and genetic animal models of Parkinson's disease, Parkinson's Dis. 2011 (2010) 951709.
[9] S. Hunot, F. Boissiere, B. Faucheux, B. Brugg, A. Mouatt-Prigent, Y. Agid, E.C. Hirsch, Nitric oxide synthase and neuronal vulnerability in Parkinson's disease, Neuroscience 72 (1996) 355–363.
[10] M. Inden, K. Takata, K. Nishimura, Y. Kitamura, E. Ashihara, K. Yoshimoto, H. Ariga, O. Honmou, S. Shimohama, Therapeutic effects of human mesenchymal and hematopoietic stem cells on rotenone-treated parkinsonian mice, J. Neurosci. Res. 91 (2013) 62–72.
[11] S.U. Kim, I.H. Park, T.H. Kim, K.S. Kim, H.B. Choi, S.H. Hong, J.H. Bang, M.A. Lee, I.S. Joo, C.S. Lee, Y.S. Kim, Brain transplantation of human neural stem cells transduced with tyrosine hydroxylase and GTP cyclohydrolase 1 provides functional improvement in animal models of Parkinson disease, Neuropathology 26 (2006) 129–140.
[12] Y.J. Kim, H.J. Park, G. Lee, O.Y. Bang, Y.H. Ahn, E. Joe, H.O. Kim, P.H. Lee, Neuroprotective effects of human mesenchymal stem cells on dopaminergic neurons through anti-inflammatory action, Glia 57 (2009) 13–23.
[13] C. Lanza, S. Morando, A. Voci, L. Canesi, M.C. Principato, L.D. Serpero, G. Mancardi, A. Uccelli, L. Vergani, Neuroprotective mesenchymal stem cells are endowed with a potent antioxidant effect in vivo, J. Neurochem. 110 (2009) 1674–1684.
[14] W. Pan, W.A. Banks, M.B. Fasold, J. Bluth, A.J. Kastin, Transport of brain-derived neurotrophic factor across the blood-brain barrier, Neuropharmacology 37 (1998) 1553–1561.
[15] H.J. Park, P.H. Lee, O.Y. Bang, G. Lee, Y.H. Ahn, Mesenchymal stem cells therapy exerts neuroprotection in a progressive animal model of Parkinson's disease, J. Neurochem. 107 (2008) 141–151.
[16] G. Paxinos, C. Watson, The Rat Brain in Streotaxic Coordinates, 6th ed., Elsevier, London, 2009.
[17] M. Quik, M. O'Neill, X.A. Perez, Nicotine neuroprotection against nigrostriatal damage: importance of the animal model, Trends Pharmacol. Sci. 28 (2007) 229–235.
[18] J.A. Rodriguez-Gomez, J.Q. Lu, I. Velasco, S. Rivera, S.S. Zoghbi, J.S. Liow, J.L. Musachio, F.T. Chin, H. Toyama, J. Seidel, M.V. Green, P.K. Thanos, M. Ichise, V.W. Pike, R.B. Innis, R.D. McKay, Persistent dopamine functions of neurons derived from embryonic stem cells in a rodent model of Parkinson disease, Stem Cells 25 (2007) 918–928.
[19] H. Sauer, W.H. Oertel, Progressive degeneration of nigrostriatal dopamine neurons following intrastriatal terminal lesions with 6-hydroxydopamine: a combined retrograde tracing and immunocytochemical study in the rat, Neuroscience 59 (1994) 401–415.
[20] S. Shimohama, H. Sawada, Y. Kitamura, T. Taniguchi, Disease model: Parkinson's disease, Trends Mol. Med. 9 (2003) 360–365.
[21] S. Suzuki, J. Kawamata, T. Matsushita, A. Matsumura, S. Hisahara, K. Takata, Y. Kitamura, W. Kem, S. Shimohama, 3-[(2,4-Dimethoxy)benzylidene]-anabaseine dihydrochloride protects against 6-hydroxydopamine-induced parkinsonian neurodegeneration through alpha7 nicotinic acetylcholine receptor stimulation in rats, J. Neurosci. Res. 91 (2013) 462–471.
[22] F. Wang, T. Yasuhara, T. Shingo, M. Kameda, N. Tajiri, W.J. Yuan, A. Kondo, T. Kadota, T. Baba, J.T. Tayra, Y. Kikuchi, Y. Miyoshi, I. Date, Intravenous administration of mesenchymal stem cells exerts therapeutic effects on parkinsonian model of rats: focusing on neuroprotective effects of stromal cell-derived factor-1alpha, BMC Neurosci. 11 (2010) 52.
[23] M. Wirenfeldt, R. Clare, S. Tung, A. Bottini, G.W. Mathern, H.V. Vinters, Increased activation of Iba1+ microglia in pediatric epilepsy patients with Rasmussen's

encephalitis compared with cortical dysplasia and tuberous sclerosis complex, Neurobiol. Dis. 34 (2009) 432–440.
[24] T. Yanagida, H. Takeuchi, Y. Kitamura, K. Takata, H. Minamino, T. Shibaike, J. Tsushima, K. Kishimoto, H. Yasui, T. Taniguchi, S. Shimohama, Synergistic effect of galantamine on nicotine-induced neuroprotection in hemiparkinsonian rat model, Neurosci. Res. 62 (2008) 254–261.
[25] W. Zheng, O. Honmou, K. Miyata, K. Harada, J. Suzuki, H. Liu, K. Houkin, H. Hamada, J.D. Kocsis, Therapeutic benefits of human mesenchymal stem cells derived from bone marrow after global cerebral ischemia, Brain Res. 1310 (2010) 8–16.